

Original paper

Litho-geochemistry and Sr–Nd isotopic composition of Neoproterozoic metasedimentary rocks of the Teplá Crystalline Complex, western Bohemian Massif: a geotectonic interpretation

Jiří FIALA^{1*}, Friedhelm HENJES-KUNST², Hiltrud MÜLLER-SIGMUND³, Zdeněk VEJNAR¹

¹ Institute of Geology, Academy of Sciences of the Czech Republic, v.v.i., Rozvojová 135, 165 02 Prague 6, Czech Republic; fiala@gli.cas.cz

² Bundesanstalt für Geowissenschaften und Rohstoffe, Geozentrum Hannover, Stilleweg 230655 Germany

³ Institut für Geo- und Umweltnaturwissenschaften, Universität Freiburg in Breisgau, Tannenbacher Str. 4, 79106 Germany

*Corresponding author



Clastic metasedimentary rocks from the Teplá Crystalline Complex (western Bohemian Massif) were analysed for major and trace elements, Sr and Nd isotopes. The metamorphic grade of these rocks of presumed Neoproterozoic protolith age increases from SE to NW from very low-grade to amphibolite-facies conditions. Geochemistry indicates that the sedimentary protoliths for the whole sequence consisted of immature (pelitic) greywackes chiefly derived from an ensialic island arc. No significant changes in composition from the lowest to the highest grade or across the strike of isograds were observed. Chemical variations between original slates and greywackes within a single locality often considerably exceed the variation among samples of different metamorphic grades or of different geographic positions. The prevailing REE spectra with distinct negative Eu anomalies show a close similarity with those of modern turbidites from ensialic island arcs. Several samples without any Eu anomaly resemble the REE patterns of less differentiated island arc andesites. LREE leaching under oxidizing conditions is suggested by several REE patterns with positive Ce anomalies. The Sm–Nd model ages T_{DM} of samples with Ce positive anomalies are higher (T_{DM} 1.8–2.0 Ga) than those of all other samples (T_{DM} = 1.1–1.5 Ga). Initial Sr isotopic ratios for all samples are fairly constant and compatible with an assumed dominance of isotopically less evolved detrital material. Geochemical characteristics of the clastic metasediments of the Teplá Crystalline Complex are thus consistent with a model of incorporation and preservation of arc-derived sediments in a Cadomian accretionary wedge.

Keywords: metasedimentary rocks, geochemistry, Sr–Nd isotopes, provenance, Teplá Crystalline Complex, Bohemian Massif

Received: 13 February 2014; **accepted:** 12 November 2014; **handling editor:** J. Žák

1. Introduction

Geodynamic models for the crystalline basement in the western Bohemian Massif concentrated mostly on reconstructing the Variscan convergence of separate geological units since the pioneering work of Weber and Behr (1983). A litho-geochemical approach to the study of selected meta-psammopelitic lithologies in the Bohemian Massif (Jakeš et al. 1979; Mrázek 1984; Čadková and Mrázek 1987; Matějka 1988) as in other segments of the Variscan orogen (Müller 1989; Wimmenauer 1991) supplied initial valuable comparative data. Several detailed structural (Hajná et al. 2010, 2013) and litho-geochemical (Drost et al. 2004, 2007) studies of the Barrandian unmetamorphosed or anchimetamorphosed Neoproterozoic sediments and volcanics appeared in the last decade. However, no systematic studies in litho-geochemistry as yet exist in the low- to high-metamorphosed western part of the Teplá–Barrandian Unit, referred to as the Teplá Crystalline Complex (TCC).

The results of the present studies on metapelites and metapsammites of the TCC allow a comparison with data

on similar rocks of the adjacent sequences of Barrandian Neoproterozoic on the one hand and with its presumed tectonometamorphic equivalent, the Erbsdorf–Vohens-straß Zone (ZEV), on the other. The ZEV is a medium-pressure unit positioned at the westernmost border of the Bohemian Massif in which the KTB superdeep borehole was located (Weber and Vollbrecht 1986).

2. Geology and metamorphism of the Teplá Crystalline Complex

The TCC represents a segment of Neoproterozoic rocks comparable to those of the Barrandian area, but affected by medium-pressure regional metamorphism. In the SE, the boundary of the TCC against the Barrandian Neoproterozoic is conventionally set to the biotite isograd (Fig. 1). The NW boundary of the TCC usually defines the SE termination of the Mariánské Lázně Complex (MLC), delineated by a continuous amphibolite band. In the N, the MLC is thrust over low-pressure/medium-

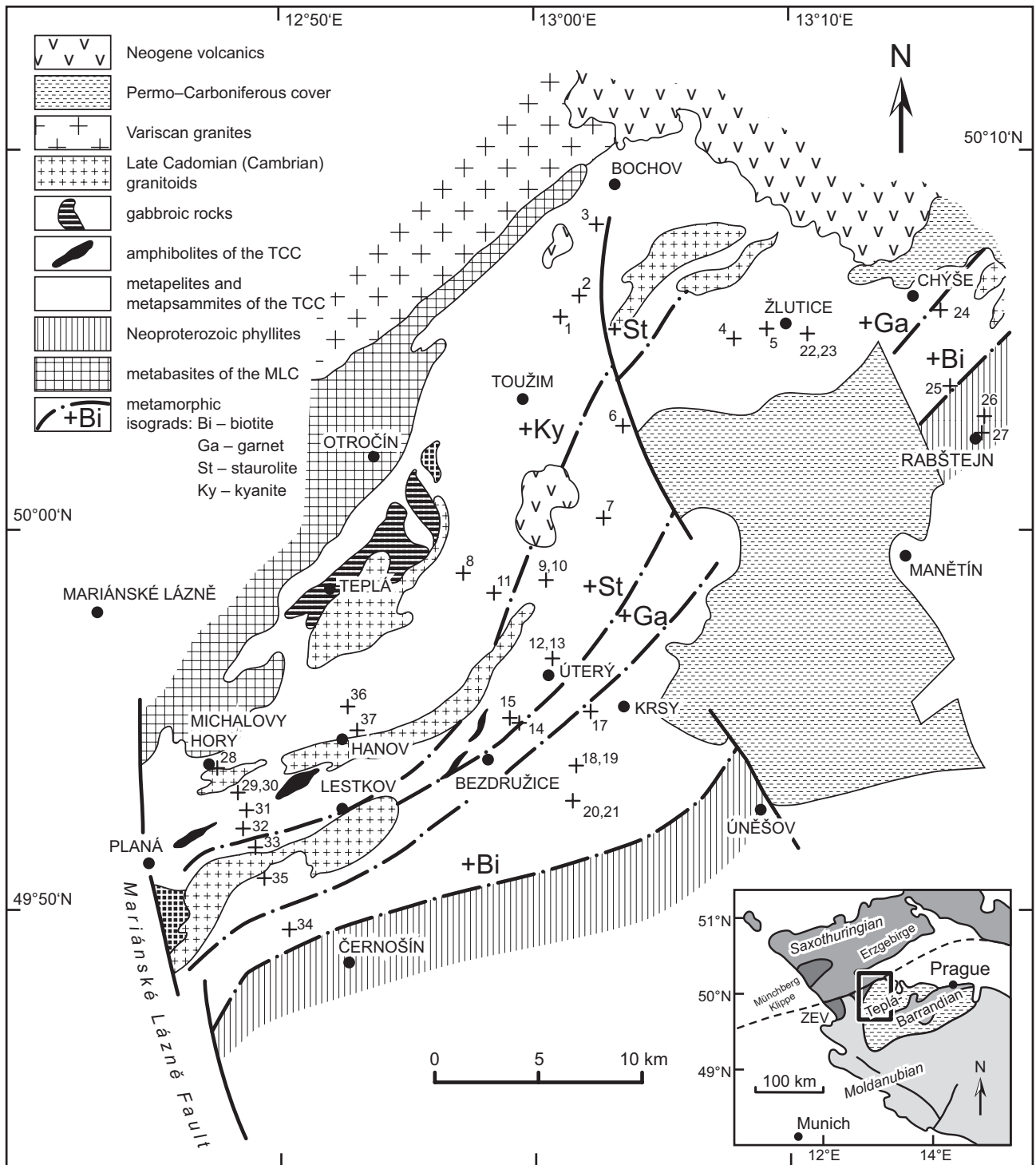


Fig. 1 Sample location and geology of the studied part of the TCC, for orientation see inset. Numbered points correspond to those in Tab. 1

temperature Saxothuringian metamorphic rocks (Kachlík 1993, 1994). The MLC thus forms the boundary between the Saxothuringian and the Teplá–Barrandian units. A similar but less distinct tectonic contact exists in the SE, where medium-pressure metamorphic rocks of the TCC are thrust toward the NW over metagabbros and am-

phibolites of the MLC (Matte et al. 1990; Zulauf 1997). Beard et al. (1995) interpreted the MLC as an exotic metaophiolite unit with its own specific lithological and metamorphic characteristics. Its emplacement is believed to have occurred during the Variscan collision between the Saxothuringian and Teplá–Barrandian units. This concept

was challenged by Štědrá et al. (2002) and Timmermann et al. (2004, 2006). The former study examined coronitic metagabbros occurring as minor bodies within the MLC and in the paragneiss and orthogneiss of the TCC. Some metagabbros caused contact metamorphism of the host rocks, and their emplacement age of 496 ± 1 Ma (Bowes and Aftalion 1991) documents the juxtaposition of the MLC and TCC prior to late Cambrian times. The latter studies obtained U–Pb zircon ages from the MLC rocks, which fall into two age groups, *c.* 540 Ma and *c.* 380 Ma. The late Cadomian age was interpreted to reflect the crystallization of the MLC oceanic protolith whereas the latter one reflects the Variscan metamorphism and decompression melting. Regional metamorphism of the TCC shows a distinct NW-oriented gradient (Kratochvíl et al. 1951) defined by tectonically reduced biotite, garnet, staurolite and kyanite zones (Fig. 1). Recent studies of the metamorphic evolution distinguished both Cadomian and Variscan Barrovian-type metamorphic overprints:

(1) To the NW of the staurolite isograd, the Cambrian granitoids have been pervasively deformed into the mylonitic Teplá and Hanov orthogneisses (Zulauf 1997; Dörr et al. 1998), whereas the Lestkov granitoid, largely situated in the garnet zone, does not show a pervasive mylonitic fabric.

(2) Variscan garnet developed in pressure shadows behind Cadomian garnet (Zulauf 1997).

(3) Variscan kyanite replaces andalusite in early Ordovician pegmatites (Žáček 1994; Glodny et al. 1998).

(4) Staurolite replaces cordierite in the northern contact aureole of the Lestkov granitoid (Cháb and Žáček 1994), indicating that the staurolite isograd reflects the Variscan cycle.

(5) The ^{39}Ar – ^{40}Ar and K–Ar dating of hornblende and white mica from the TCC yielded ages of 383 Ma and 366–371 Ma, respectively (Kreuzer et al. 1992; Dallmeyer and Urban 1998). Hornblende ages suggest a Devonian temperature of more than *c.* 500 °C for the northwestern part of the TCC, assuming such a closure temperature for the K–Ar isotopic system of hornblende (Zulauf et al. 2004).

Investigations into the crystallization–deformation relationships in the TCC indicate that the biotite and garnet isograds of Cháb and Žáček (1994) (Fig. 1) reflect the Cadomian orogeny, whereas the staurolite and kyanite isograds are Variscan in age. Variscan biotite and garnet appear immediately to the NW of the Cadomian garnet isograd. To the SE of the garnet isograd, the Variscan deformation occurred under retrograde metamorphic conditions as compared to the Cadomian fabrics (Zulauf et al. 2004).

3. Lithology, lithostratigraphy and age of the Teplá Crystalline Complex

The existing knowledge of the lithology of the TCC protolith is mostly based on geological mapping (Vejnar et

al. 1962) and studies of metamorphic processes (Žáček and Cháb 1993; Cháb and Žáček 1994) and is further expanded by this paper.

The dominant lithological type are finely laminated psammo–pelitic rhythmites with isolated slaty greywacke bodies and rare greywackes that form alternating bodies tens of centimeters to meters in thickness. The absence of thicker greywacke bodies, the scarcity of basic volcanoclastic sediments (Fig. 1) and only an isolated occurrence of black shales suggest an originally lithologically monotonous succession (Holubec 1966).

Lithostratigraphic correlation of the TCC with the Barrandian Neoproterozoic is only conventional. It is supported by a similar lithofacies development of the two units, particularly along their contact, *i.e.*, along the biotite isograd. Although various lithostratigraphic schemes have been proposed for the Barrandian Neoproterozoic, including the TCC (Kettner 1917; Röhlich 1965; Holubec 1966; Cháb and Pelc 1968, 1973; Cháb 1978; Mašek and Zoubek 1980; Kříbek et al. 2000; Mašek 2000; Röhlich 2000; Lang 2000), recent studies of Hajná et al. (2010, 2011, 2012 and 2013) suggested that the central and NW parts of the Teplá–Barrandian unit represent a fragment of an accretionary wedge of the Avalonian–Cadomian belt, which developed along the northern active margin of Gondwana during the Late Neoproterozoic. This interpretation implies that the various component units (commonly fault-bounded) of the presumed wedge may not exhibit mutual stratigraphic relationships as straightforward as previously thought. Nevertheless, the TCC can be correlated with a lithologically similar NW part of the Barrandian Neoproterozoic, referred to as the Kralovice–Rakovník Belt (Röhlich 1965; Hajná et al. 2010, 2011), with the difference being that the TCC is progressively metamorphosed up to the amphibolite facies.

The age constraints for the TCC metasedimentary rocks are the emplacement ages of the metagranitoids and metapegmatites. The TCC Cambrian (meta-)granitoids (the Lestkov Massif, the Teplá and Hanov orthogneisses) yielded U–Pb zircon intrusive ages of *c.* 513 Ma (Dörr et al. 1998), the metapegmatites gave U–Pb columbite, garnet, monazite and zircon as well as Rb–Sr muscovite ages of *c.* 480 Ma (Košler et al. 1997; Glodny et al. 1998). These data thus provide an upper limit for age of deposition of metasedimentary rocks of the TCC, most probably pointing to Neoproterozoic to early Cambrian. Paper by Dörr et al. (2002) summarized the geochronological evolution of the Teplá–Barrandian Unit in early Cambrian to Neoproterozoic times.

4. Methods and sample description

The TCC metasedimentary rocks were sampled along a cross-section from very low-grade chlorite–sericite

Tab. 1 List of samples with their WGS coordinates

No.	Description	Variety	Location	N	E
1	Two-mica paragneiss with Grt, Ky and Sil	shl/shl	Abandoned quarry in a weekend-house settlement 1.5 km NNE of Kojšovice	50.0923	13.0136
2	Two-mica paragneiss with Grt, Ky and Pl porphyroblasts	grw/grw	Roadcut at the Toužim–Bochov road, S periphery of Kozlov	50.1034	13.0256
3	Two-mica paragneiss with Grt and micaceous stripes	grw/grw	Rocky outcrop in the valley of the Bochov Stream, 3 km SSW of Bochov	50.1320	13.0376
4	Muscovite-rich paragneiss with Grt and Chl	shl/shl	Rocky outcrops below the dam W of Žlutice	50.0854	13.1291
5	Two-mica paragneiss with Grt and Chl	shl/shl	Rocky outcrops in the valley of Střela River 0.5 km W of Žlutice	50.0876	13.1504
6	Micaschist with Grt	grw/grw	Outcrop on the elevation 1 km S of the Smilov railway station E of Toužim	50.0445	13.0515
7	Micaschist with Grt, St and Pl poikiloblasts	grw/grw	Outcrop 2 km NW of Bezvěrov at the road to Toužim	50.0080	13.0374
8	Two-mica paragneiss with Grt, St, Ky and Pl poikiloblasts	shl/grw	Outcrop 0.8 km E of Dobrá Voda E of Teplá	49.9885	12.9512
9	Biotite-rich micaschist with Grt	grw/grw	Quarry on elevation 1.5 km S of Branišov above the Úterý Stream valley	49.9781	12.9970
10	Micaschist with Grt and St	shl/shl	For the location see No. 9	49.9781	12.9970
11	Micaschist with Grt and St	shl/shl	Roadcut of the forest road 1 km NW of Vidžín	49.9768	12.9708
12	Biotite micaschist with Grt, prh and graphite substance	grw/grw	Outcrop on the N periphery of Úterý, left bank of the Úterý Stream	49.9430	13.0039
13	Micaschist with Grt and St	shl/shl	For the location see No.12	49.9430	13.0039
14	Micaschist with Grt	shl/shl	Roadcut 2 km SSW of Úterý at the road to Bezdrůžice	49.9207	12.9898
15	Biotite micaschist with Grt, Po and graphite substance	grw/grw	Outcrop 2.5 km SSW of Úterý at the road to Bezdrůžice	49.9210	12.9851
17	Phyllite with Bt, Qtz clasts and volcanics fragments	grw/grw	Outcrop at the road between Úterý and Krsy in the Dolský Stream valley	49.9221	13.0306
18	Phyllite with Bt	shl/shl	Outcrop in the Úterý Stream valley 1.5 km W of Ostrov near Bezdrůžice	49.9002	13.0216
19	Phyllite with Bt and Qtz–Pl clasts	grw/grw	For the location see No.18	49.9002	13.0216
20	Phyllite with sporadic Bt	slt/sltshl/shl	Outcrop at Starý Mlýn on the Úterý Stream S of the Krsy–Bezdrůžice road	49.8880	13.0194
21	Phyllite with Bt	grw/shl	For the location see No. 20	49.8880	13.0194
22	Micaschist with Grt and Chl	shl/shl	Outcrop at the road 1 km SE of Žlutice	50.0899	13.1742
23	Biotite micaschist with Grt	grw/grw	For the location see No. 22	50.0899	13.1742
24	Micaschist with sporadic Grt	shl/grw	Outcrop in the Střela River valley 1 km SE of Chýše	50.1020	13.2635
25	Phyllite with sporadic Bt, silky glitter	shl/shl	Outcrop in the Střela River valley 0.5 km ESE of Jablonné	50.0652	13.2747
26	Roofing phyllite with Po	shl/shl	Abandoned quarry 1 km NE of Rabštejn	50.0557	13.2995
27	Roofing phyllite with Po	shl/shl	Abandoned quarry at Rabštejn	50.0471	13.2959
28	Two-mica paragneiss with Grt, Ky and Sil	shl/shl	Outcrop on the E periphery of Michalovy Hory, left bank of the Kosi Stream	49.9001	12.7911
29	Two-mica paragneiss with Grt, Ky and Sil	shl/shl	Outcrop 2 km SE of Michalovy Hory, left bank of the Kosi Stream	49.8881	12.8064
30	Two-mica paragneiss with Grt	grw/grw	For the location see No. 29	49.8881	12.8064
31	Two-mica paragneiss with Ky	shl/shl	Outcrop 3 km SE of Michalovy Hory, left bank of the Kosi Stream	49.8803	12.8105
32	Two-mica paragneiss with Grt, St and Ky	shl/shl	Outcrop on the left bank of the Kosi Stream 3.5 km E of Planá	49.8730	12.8097
33	Micaschist wit Grt	grw/grw	Outcrop on the promontory, left bank of the Kosi Stream, 4 km E of Planá	49.8683	12.8164
34	Phyllite with Bt and Qtz-Pl clasts	grw/grw	Outcrop on left bank of the Kosi Stream at the Stříbro–Planá road	49.8277	12.8402
35	Micaschist with Grt, contact-metamorphozed to Bt-hornfels	grw/grw	Outcrop on the right bank of the Kosi Stream, E periphery of Křínov	49.8538	12.8194
36	Two-mica paragneiss with Grt and Ky nodules	shl/shl	Outcrop on the left bank of the Hadovka Stream at the Lestkov–Teplá road	49.9251	12.8761
37	Two-mica paragneiss with Grt and Ky	shl/shl	Outcrop on the left bank of the Hadovka Stream 1 km NE of Hanov	49.9123	12.8856

Rock types: shl – metashale, grw – metagreywacke – megascopic classification/chemical classification according to Fig. 2
 Mineral abbreviations are after Kretz (1983)

phyllites to amphibolite-facies kyanite–garnet gneisses (Fig. 1). A total of 36 samples, *c.* 2–3 kg in weight, were collected from outcrops and quarries. Table 1 contains overview of the rock types, location of sampling sites and their geographic coordinates. Sampled lithologies comprised either metashale (shl) or metagreywacke (grw). The samples were homogenized by standard methods at the Institute of Geology Academy of Sciences of the Czech Republic (AS CR). The XRF analyses for major and trace elements were performed by one of the authors (Müller-Sigmund) on a PHILIPS PW2404 spectrometer at the Institute of Earth and Environmental Sciences, Albert-Ludwig University, Freiburg in Breisgau, Germany, using methods described in Norrish and Chappell (1977). The REE analytical procedure (Povondra et al. 1968) consists in sample decomposition in a mixture of concentrated nitric and hydrofluoric acids. Lanthanide fluorides were converted into perchlorates by repeated evaporation with perchloric acid. Dissolved samples were transferred on ion exchange resin and the REE were selectively eluted, getting rid of other matrix cations. Collected fractions containing lanthanides were analysed

by ICP-OES method (P. Foch, Czech Geological Survey, Prague in collaboration with P. Povondra, Faculty of Science, Charles University, Prague).

The Rb–Sr and Sm–Nd isotopic determinations were carried out by another author (Henjes-Kunst) at the Federal Institute for Geosciences and Natural Resources (BGR). Sample powders were mixed with ^{87}Rb – ^{84}Sr and ^{147}Sm – ^{148}Nd spikes and dissolved in a micro-wave furnace in a two-steps procedure (1st step: concentrated HF–HNO₃; 2nd step: 6M HCl). Rubidium, Sr, and the lanthanides were separated on standard cation-exchange columns. Samarium and Nd were isolated from each other and adjacent REE in separate columns using HDEHP-coated Teflon powder (Cerrai and Testa 1963). The isotopic composition of Rb was measured on a VG-Micro-mass MM30 single-collector mass spectrometer; those of Sr, Sm and Nd on a Finnigan MAT 261 multi-collector mass spectrometer equipped with five Faraday cups. Neodymium isotopic ratios were normalized to $^{146}\text{Nd}/^{144}\text{Nd} = 0.7219$ and are reported relative to $^{143}\text{Nd}/^{144}\text{Nd} = 0.511860$ for the La Jolla Nd standard. Strontium isotopic ratios were normalized to $^{86}\text{Sr}/^{88}\text{Sr} = 0.1194$ and are reported relative to $^{87}\text{Sr}/^{86}\text{Sr} = 0.710245$

Tab. 2 Major-element data for the Teplá Crystalline Complex metasediments [wt. %]

No.	1	2	3	4	5	6	7	8	9	10	11	12	13	14	15	17	18	19
SiO ₂	66.85	64.89	71.40	65.19	62.81	72.50	66.40	73.33	66.71	68.29	64.30	69.79	67.33	69.53	68.79	65.11	62.81	70.07
TiO ₂	0.68	0.86	0.72	0.71	0.75	0.69	0.67	0.62	0.69	0.69	0.74	0.65	0.78	0.71	0.74	0.71	0.78	0.66
Al ₂ O ₃	15.28	16.90	13.75	16.23	17.53	13.49	15.89	12.96	15.83	15.74	17.23	14.09	16.93	15.29	14.90	15.64	17.19	14.12
FeO(t)	5.35	5.56	3.82	5.44	6.11	3.80	4.88	3.68	4.69	4.63	5.47	3.56	4.22	3.77	4.13	4.87	5.88	4.43
MnO	0.10	0.09	0.05	0.10	0.11	0.08	0.07	0.08	0.11	0.08	0.10	0.06	0.05	0.04	0.04	0.09	0.08	0.05
MgO	2.15	2.18	1.40	2.24	2.57	1.34	1.98	1.53	1.62	1.67	2.05	1.36	1.73	1.60	1.62	1.87	2.45	1.87
CaO	0.95	1.42	0.83	0.91	1.00	1.13	2.49	0.84	1.57	0.78	0.89	2.58	0.61	0.66	1.55	1.85	0.27	0.22
Na ₂ O	2.72	2.90	3.78	2.76	2.51	3.08	3.24	2.53	5.04	3.00	3.20	4.27	2.07	2.41	5.11	4.14	3.28	3.23
K ₂ O	2.63	2.18	2.23	2.93	3.10	1.87	1.89	2.13	1.60	2.71	2.87	0.98	3.29	2.68	1.30	1.99	2.77	2.02
P ₂ O ₅	0.12	0.07	0.10	0.12	0.13	0.11	0.13	0.10	0.29	0.11	0.14	0.28	0.07	0.09	0.10	0.15	0.17	0.14
H ₂ O ⁺	1.60	1.92	0.80	1.75	2.21	0.88	0.84	1.10	0.83	1.44	1.49	0.55	2.14	1.94	0.51	1.53	2.93	1.98
CO ₂	0.54	0.79	0.79	0.27	0.36	0.38	0.09	0.67	0.00	0.37	0.36	0.97	0.66	0.47	0.18	0.77	0.61	0.51
Σ	98.97	99.76	99.67	98.65	99.19	99.35	98.57	99.57	98.98	99.51	98.84	99.14	99.88	99.19	98.97	98.72	99.22	99.30
No.	20	21	22	23	24	25	26	27	28	29	30	31	32	33	34	35	36	37
SiO ₂	60.14	60.79	64.91	64.81	64.00	65.27	62.43	62.62	61.97	70.80	73.57	61.93	65.21	66.21	64.53	63.03	65.40	64.86
TiO ₂	0.81	0.83	0.70	0.76	0.76	0.75	0.77	0.80	0.86	0.71	0.67	0.83	0.76	0.73	0.82	0.79	0.84	0.76
Al ₂ O ₃	18.19	18.22	16.01	16.66	16.72	17.23	16.94	17.14	18.73	14.67	12.74	18.21	17.03	15.67	15.85	16.60	16.84	17.25
FeO(t)	6.99	6.55	5.79	4.94	5.57	4.63	5.83	6.15	6.35	4.22	3.60	6.27	5.81	5.08	5.42	5.62	5.97	5.41
MnO	0.08	0.08	0.13	0.08	0.09	0.04	0.09	0.09	0.09	0.06	0.00	0.12	0.11	0.11	0.07	0.08	0.10	0.10
MgO	2.80	2.75	2.48	2.17	2.35	1.83	2.58	2.69	2.47	1.64	1.35	2.52	2.27	2.10	2.40	2.38	2.33	2.02
CaO	0.28	0.27	1.12	2.36	1.69	0.26	0.93	0.41	0.73	0.94	1.46	1.01	0.94	2.40	1.04	2.09	1.08	0.77
Na ₂ O	2.44	2.67	2.66	4.02	3.51	2.66	3.04	3.14	2.57	2.56	3.42	3.12	2.75	3.79	5.04	4.17	2.31	2.93
K ₂ O	3.48	3.40	2.69	2.13	2.46	3.27	2.88	2.83	3.47	2.40	1.59	3.17	3.01	1.92	1.54	2.08	2.81	3.00
P ₂ O ₅	0.17	0.16	0.12	0.12	0.13	0.13	0.16	0.17	0.13	0.12	0.09	0.15	0.14	0.13	0.15	0.13	0.16	0.16
H ₂ O ⁺	3.47	3.29	2.02	1.29	1.84	2.81	2.70	2.52	1.68	1.13	0.60	1.51	1.26	0.99	1.77	1.58	1.63	1.47
CO ₂	0.60	0.64	0.66	0.34	0.37	0.68	0.69	0.29	0.09	0.11	0.07	0.89	0.19	0.12	0.40	0.09	0.14	0.32
Σ	99.45	99.65	99.29	99.68	99.49	99.56	99.04	98.85	99.14	99.36	99.16	99.73	99.48	99.25	99.03	98.64	99.61	99.05

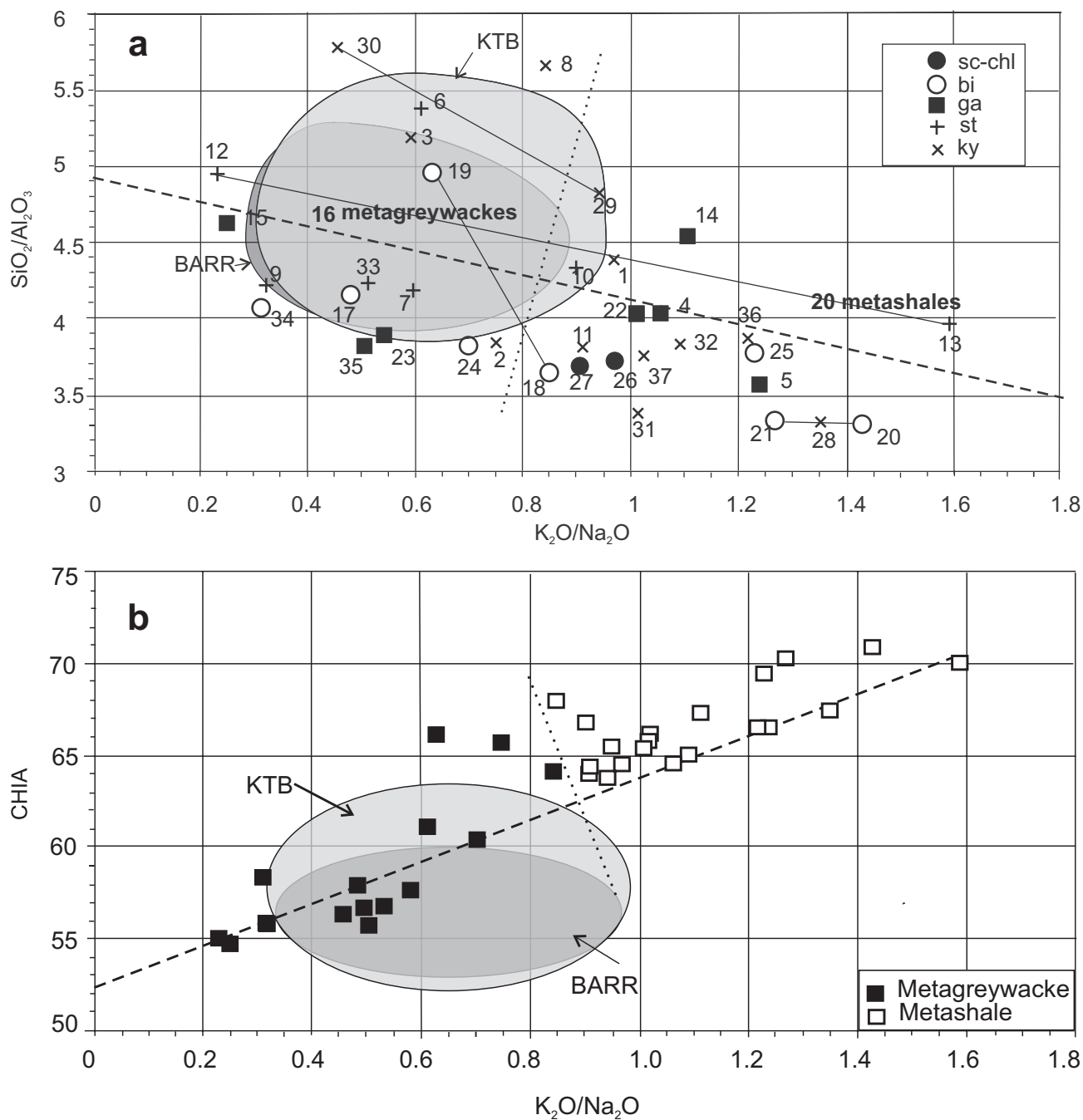


Fig. 2a – Metasedimentary rocks of the TCC in the plot of Wimmenauer (1984). Isograd affiliation of samples is: sc–chl – sericite–chlorite, bi – biotite, ga – garnet, st – staurolite, ky – kyanite. **b** – Binary plot $\text{K}_2\text{O}/\text{Na}_2\text{O}$ vs. CHIA (chemical index of alteration – Nesbit and Young 1982). The grey fields BARR – Barrandian Neoproterozoic, KTB – Superdeep borehole Windisch–Eschenbach/FRG. The dotted line – estimated boundary between metagreywacke and metashale type samples. The dashed line – regression line of all samples. Solid lines connect metagreywacke and metashale pairs from one locality.

for the SRM 987 Sr standard. Procedural blanks were less than 0.1 % of the relevant sample concentrations and are therefore negligible. Uncertainties ($\pm 2\sigma$) were 0.03 % for $^{87}\text{Sr}/^{86}\text{Sr}$, 0.06 % for $^{143}\text{Nd}/^{144}\text{Nd}$, 1 % for $^{87}\text{Rb}/^{86}\text{Sr}$ and 0.4 % for $^{147}\text{Sm}/^{144}\text{Nd}$ according to long-term measurements of the granite SARM and feldspar NBS 607 standards. Calculation of the ϵ_{Nd} values is based on $^{143}\text{Nd}/^{144}\text{Nd} = 0.512638$

and $^{147}\text{Sm}/^{144}\text{Nd} = 0.1967$ for a CHUR (Jacobsen and Wasserburg 1980). Single-stage depleted-mantle model ages $T_{\text{Nd}}(\text{DM})$ were calculated assuming $^{143}\text{Nd}/^{144}\text{Nd} = 0.513151$ and $^{147}\text{Sm}/^{144}\text{Nd} = 0.219$ for the present-day depleted-mantle reservoir and a linear Sm/Nd evolution through time. In all calculations, the IUGS-recommended constants (Steiger and Jäger 1977) were used.

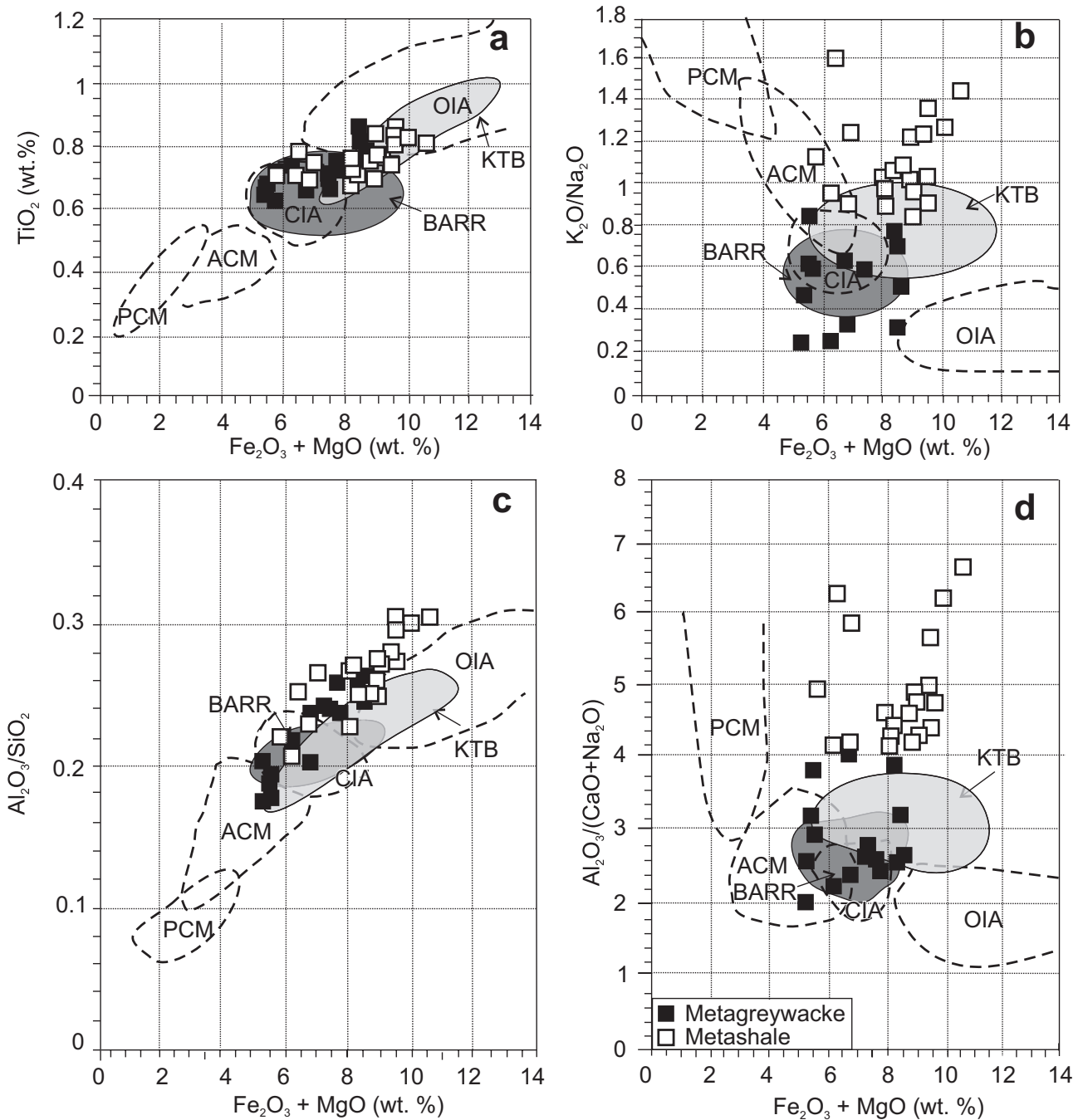


Fig. 3 Metasedimentary rocks of the TCC in the plots of Bhatia (1983). Geotectonic settings: PCM – passive continental margin, ACM – active continental margin, CIA – continental island arc, OIA – oceanic island arc.

5. Geochemistry

5.1. Major elements

The analysed metasedimentary rocks of the TCC (Tab. 2) contain 60.1 to 73.6 wt. % SiO_2 and 13.0 to 18.7 wt. % Al_2O_3 . According to $\text{K}_2\text{O}/\text{Na}_2\text{O}$ vs. $\text{SiO}_2/\text{Al}_2\text{O}_3$ (all in wt.%) classification plot of Wimmenauer (1984) (Fig. 2a), almost all the TCC samples plot in the field of grey-

wackes. The $\text{K}_2\text{O}/\text{Na}_2\text{O}$ ratio varies broadly around the median value of 0.8 from about 0.2 to 1.6, which, at the same time, represents the scatter of the greywacke–shale counterparts from a single locality (samples 12 and 13).

Individual samples in Fig. 2a display a negative trend marked by the regression line (dashed), reflecting progressive weathering and decomposition of mostly plagioclase, connected with an increase in clay mineral proportion in the primary sediment. Empirical line

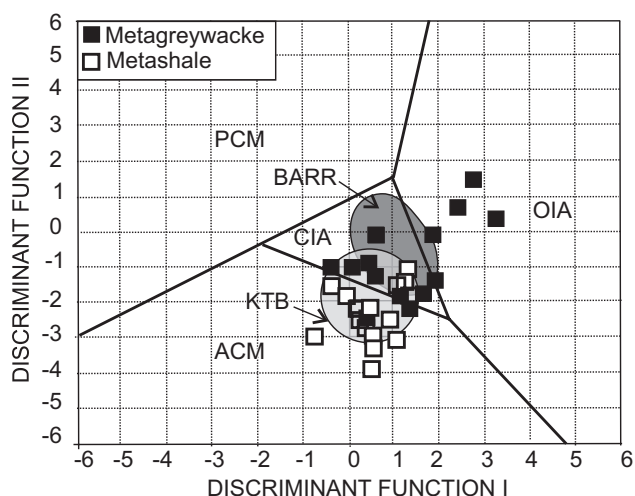


Fig. 4 Metasedimentary rocks of the TCC in the plot of discriminants scores after Bhatia (1983). For abbreviations see Fig. 3.

(dotted) in Fig. 2a separates 16 metagreywackes from 20 metashales based on field evidence. We use this division also in further projections.

No systematic compositional changes are observed from the lowest to the highest grades of metamorphism or across the strike of the isograds (Fig. 1). Variations due to sedimentary sorting within a sedimentary succession (marked sample pairs in Fig. 2a) exceed that between samples of different metamorphic grades or geographic positions.

Geochemical relationship between the TCC and the unmetamorphosed to anchimetamorphosed Barrandian Neoproterozoic metasedimentary rocks was assessed using data of Čadková et al. (1985). We prefer this geochemical database produced in a single laboratory of the Czech Geological Survey. The field “BARR” in Fig. 2a covers 90 % of data points of 50 Barrandian greywacke samples. Geochemical relation of the TCC to the similar metamorphosed monotonous sequence of the western part of the Bohemian Massif, the Erbendorf–Vohenstrauß Zone, was studied using data of Wimmenauer (1991). The field “KTB” in Fig. 2a covers 90 % of data points of 40 metagreywacke samples from the KTB superdeep borehole.

The plot of K_2O/Na_2O (in wt. %) vs. the chemical index of alteration (CHIA according to Nesbitt and Young 1982) is shown in Fig. 2b. The CHIA is defined as the molar ratio $Al_2O_3/(Al_2O_3 + K_2O + Na_2O + CaO^*) \times 100$, where CaO^* represents Ca residing only in silicate minerals (i.e., corrected for Ca in carbonates and phosphates). The TCC samples exhibit a positive trend marked by a regression line (dashed) reflecting a more intense alteration of metashale samples. The CHIA cut-off value of about 63 separates most of metagreywackes (down to 54.7) from metashales (up to 70.8). Note that the Barrandian and KTB fields (see Fig. 2a) plot within the “metagrey-

wacke” domain, i.e. that characterized by relatively low degree of alteration.

Major-element compositions of elastic sediments show systematic variations depending on the tectonic setting (Bhatia 1983). Figure 3 plots mafic components of Fe_2O_3 (total iron) + MgO in wt. % against TiO_2 (wt. %), K_2O/Na_2O , Al_2O_3/SiO_2 and $Al_2O_3/(CaO+Na_2O)$, respectively. Possible tectonic settings are as follows: passive continental margin (PCM), active continental margin (ACM), continental-island arc (CIA) and oceanic-island arc (OIA). In Fig. 3a, the studied metagreywackes plot mostly to the CIA field, whereas metashales shift slightly to the OIA field. The latter is probably due to relative mafic component enrichment in the clayey phase of the primarily more altered shale variety. The Barrandian greywackes cover the CIA field whereas the KTB ones straddle the boundary of the adjacent OIA field. Figures 3b, d document a conspicuous mobility of alkalis and CaO due to weathering and decomposition processes. In both cases, the less altered greywackes plot in the CIA field, whereas in Fig. 3b, the more strongly altered shales fall outside any of the fields defined. In the above-mentioned figures, the KTB metagreywacke data shift markedly in the same sense as the TCC metashales. Plots with less mobile elements (Fig. 3a, c) produce more compact pictures, which holds particularly for the Barrandian greywackes probably spared of stronger alteration.

Taken together, the set of major-element plots in Fig. 3 suggest a mostly CIA provenance for the studied samples, as well as for the KTB and BARR greywacke sediments. The same conclusion comes from the plot of major-element based discriminant functions after Bhatia (1983) (Fig. 4). All the presented plots were set up by analysing “sandstones”, in fact mostly by greywackes in island-arc settings (Bhatia 1983). For chemically more altered shale lithologies, the discrimination diagrams are more or less invalid.

5.2. Binary and ternary plots based on trace elements

Trace-element data of the analysed TCC metasediments are given in Tab. 3. Various plots are used to discriminate the provenance of the sedimentary protolith (Figs 5–6). In the ternary Co–Th–Zr/10 plot of Bhatia and Crook (1986) (Fig. 5a), the TCC metasediments and Barrandian greywackes concentrate in the continental-island arc area (in the KTB data set, Co analyses are missing). The Sc–Th–Zr/10 plot (Fig. 5b) provides a similar picture. The KTB field is also missing, because of the lack of Sc data. The La vs. Th plot (Fig. 6a) points unequivocally to a CIA setting only for the Barrandian greywackes, whereas the TCC and KTB metasediment data fall mostly outside the delimited fields. The “normal” La/Th ratio of the

Tab. 3 Trace-element data (except REE) for the Teplá Crystalline Complex metasediments [ppm]

No.	1	2	3	4	5	6	7	8	9	10	11	12	13	14	15	17	18	19
Rb	86	68	83	96	95	61	65	68	68	87	96	50	98	81	41	66	89	64
Sr	122	190	145	135	131	157	231	127	204	128	148	170	110	84	135	223	120	122
Ba	574	713	465	620	572	486	387	505	246	533	527	167	723	675	432	420	554	535
Pb	14	17	14	21	24	12	12	16	27	20	19	13	15	16	17	19	17	14
Cu	29	27	8	28	36	5	18	12	4	12	22	19	20	18	3	23	25	18
Zn	107	100	81	99	124	67	61	56	78	82	89	104	85	67	33	77	107	77
Ga	17	19	13	18	20	13	17	12	13	17	20	11	19	17	12	15	18	14
Nb	9	10	8	9	10	7	3	7	8	8	10	7	10	8	7	5	11	7
Zr	174	261	265	176	171	250	145	217	216	217	193	229	198	210	213	188	197	199
Hf	6	6	7	5	5	5	4	6	6	6	7	6	5	5	6	5	4	5
Th	7.7	13.8	8.4	8.2	8.1	8.0	5.1	6.5	8.6	8.2	9.2	7.6	8.4	7.7	7.9	6.4	8.7	7.2
U	3.2	3.1	3.3	3.1	2.9	2.7	1.4	2.6	3.1	3.1	3.3	3.0	3.9	3.1	3.1	2.1	1.7	1.8
Y	30	55	28	32	30	26	23	26	29	30	30	29	33	31	33	24	29	23
Sc	13	14	12	16	16	13	15	13	15	15	15	16	15	15	12	14	14	14
V	147	154	111	164	165	106	114	106	124	133	144	101	174	146	141	114	163	129
Cr	81	70	58	89	88	68	78	64	63	62	78	46	76	58	66	49	85	66
Co	20	11	5	7	16	4	13	4	12	10	13	11	3	3	9	12	16	11
Ni	45	14	13	25	38	15	26	14	24	25	31	48	6	5	21	18	36	27
La	37.9	57.9	33.8	36.5	34.1	31.3	26.6	30.6	31.0	31.8	35.6	30.8	37.0	31.9	33.0	28.5	16.1	11.1
Th/Sc	0.59	0.99	0.70	0.51	0.51	0.62	0.34	0.50	0.57	0.54	0.61	0.48	0.56	0.51	0.66	0.46	0.62	0.52
Zr/Sc	13.4	18.6	22.1	11.0	10.7	19.2	9.7	16.7	14.4	14.5	12.9	14.3	13.2	14.0	17.8	13.4	14.1	14.2
Th/U	2.40	4.40	2.52	2.66	2.82	2.96	3.57	2.49	2.76	2.68	2.79	2.56	2.19	2.50	2.55	3.11	4.98	4.09
Cr/V	0.55	0.45	0.52	0.54	0.53	0.64	0.68	0.60	0.51	0.47	0.54	0.46	0.44	0.40	0.47	0.43	0.52	0.51
Y/Ni	0.66	3.90	2.16	1.28	0.80	1.71	0.89	1.83	1.21	1.19	0.97	0.60	5.49	6.17	1.56	1.33	0.81	0.86
La/Sc	2.91	4.13	2.81	2.28	2.13	2.41	1.77	2.35	2.07	2.12	2.38	1.92	2.46	2.13	2.75	2.03	1.15	0.80
Rb/Sr	0.70	0.36	0.57	0.71	0.73	0.39	0.28	0.54	0.33	0.68	0.65	0.29	0.89	0.96	0.30	0.30	0.74	0.52
Cr/Ni	1.80	5.00	4.46	3.56	2.32	4.53	3.00	4.57	2.63	2.48	2.52	0.96	12.67	11.60	3.14	2.72	2.36	2.44

No.	20	21	22	23	24	25	26	27	28	29	30	31	32	33	34	35	36	37
Rb	110	104	91	67	78	108	96	93	122	78	55	107	99	69	51	69	94	103
Sr	95	99	146	305	203	115	121	89	125	140	177	150	123	297	252	289	132	123
Ba	730	697	602	495	611	665	596	598	625	560	404	565	518	460	623	480	593	525
Pb	18	19	26	26	24	31	26	15	18	22	22	26	24	19	12	14	13	22
Cu	28	25	19	10	12	18	31	30	27	16	10	21	3	8	14	18	0	8
Zn	125	114	109	82	92	101	107	112	118	87	69	109	104	79	77	100	123	109
Ga	22	22	18	16	19	19	19	20	23	16	11	20	20	18	15	19	20	20
Nb	11	11	10	6	10	9	11	11	14	8	7	12	10	8	6	11	12	11
Zr	176	183	171	179	227	220	198	195	206	226	249	194	177	211	221	203	224	207
Hf	4	5	5	5	6	6	6	6	5	6	7	5	4	6	6	5	6	6
Th	9.0	9.3	8.5	5.7	8.5	8.5	9.5	9.3	10.2	7.9	8.0	9.4	8.4	7.2	7.3	9.3	8.7	9.6
U	2.0	1.9	2.7	1.7	2.2	2.8	3.0	2.8	3.8	3.2	2.7	3.7	3.2	2.4	2.2	2.0	3.8	3.6
Y	25	25	25	16	29	21	25	31	32	29	23	34	31	25	24	22	34	34
Sc	16	11	13	15	13	14	14	13	16	16	14	12	17	13	14	15	14	14
V	188	196	158	135	131	150	176	180	185	128	110	172	159	126	142	174	168	161
Cr	99	100	81	74	67	63	94	84	91	84	70	104	78	65	66	92	75	90
Co	18	11	16	9	11	8	11	18	14	8	6	14	13	13	15	16	16	12
Ni	47	45	39	11	23	15	42	44	34	26	16	29	35	20	20	42	37	28
La	16.9	11.6	33.2	9.3	36.4	26.4	34.0	36.3	36.8	33.2	31.7	40.6	34.2	26.2	27.2	16.5	36.8	35.2
Th/Sc	0.56	0.85	0.66	0.38	0.65	0.60	0.68	0.72	0.64	0.50	0.57	0.78	0.49	0.55	0.52	0.62	0.62	0.68
Zr/Sc	11.0	16.6	13.2	11.9	17.5	15.7	14.1	15.0	12.9	14.1	17.8	16.2	10.4	16.2	15.8	13.5	16.0	14.8
Th/U	4.47	4.89	3.18	3.35	3.92	3.04	3.16	3.34	2.68	2.44	2.95	2.53	2.65	2.93	3.27	4.61	2.29	2.69
Cr/V	0.53	0.51	0.51	0.55	0.51	0.42	0.53	0.47	0.49	0.66	0.64	0.60	0.49	0.52	0.46	0.53	0.45	0.56
Y/Ni	0.54	0.56	0.63	1.44	1.27	1.39	0.60	0.70	0.95	1.11	1.43	1.18	0.89	1.23	1.22	0.53	0.91	1.22
La/Sc	1.05	1.05	2.56	0.62	2.80	1.89	2.43	2.79	2.30	2.07	2.27	3.38	2.01	2.01	1.94	1.10	2.63	2.51
Rb/Sr	1.16	1.05	0.62	0.22	0.38	0.94	0.79	1.04	0.98	0.56	0.31	0.71	0.80	0.23	0.20	0.24	0.71	0.84
Cr/Ni	2.11	2.22	2.08	6.73	2.91	4.20	2.24	1.91	2.68	3.23	4.38	3.59	2.23	3.25	3.30	2.19	2.03	3.21

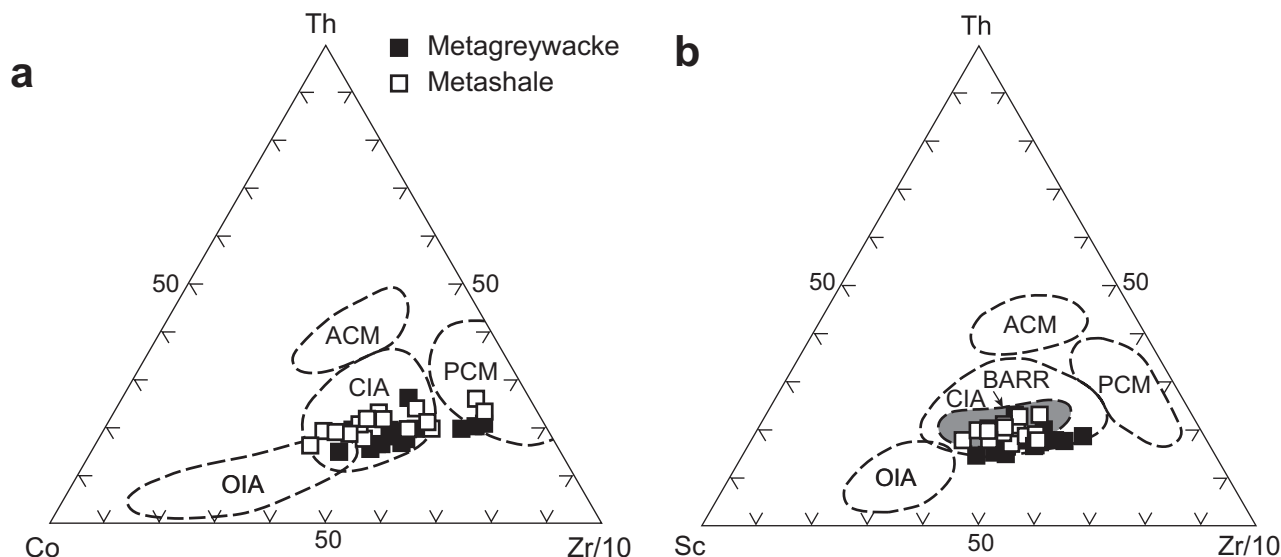


Fig. 5 Metasedimentary rocks of the TCC in the ternary plots of Bhatia and Crook (1986). For the meaning of abbreviations, see Fig 3.

pre-defined fields is ~2 whereas the majority of TCC and KTB data concentrate at La/Th ~ 4. The La/Sc vs. Ti/Zr plot of Bhatia and Crook (1986) in Fig. 6b shows again a compact picture. Almost all the TCC and Barrandian data concentrate within the CIA field (Sc data are missing in the KTB analyses). Another hint on possible sediment

provenance is presented by the Hf vs. La/Th plot of Floyd and Leveridge (1987) (Fig. 7). The so-called “acidic arc source” in this plot corresponds roughly to the CIA area in the previous plots, and the affinity of the TCC, BARR and a part of KTB data to this area is obvious. The remaining KTB data show a tendency to follow the passive margin trend (compare with Fig. 3b, d).

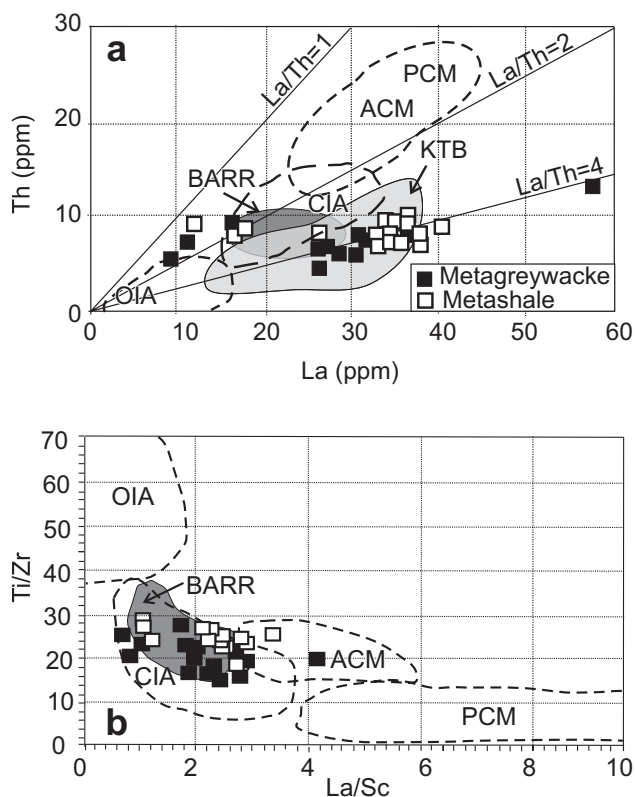


Fig. 6 Metasedimentary rocks of the TCC in the binary plots Bhatia and Crook (1986). a – La vs. Th; b – La/Sc vs. Ti/Zr. For the meaning of abbreviations, see Fig 3.

5.3. Multi-element (spider) diagrams

Figure 8 is a multi-element plot normalized to Primitive Mantle (PRM) composition after Taylor and McLennan (1985). The element order in the diagram follows the decreasing average contents in the upper continental crust (UCC) according to Taylor and McLennan (1985), except for phosphorus, which is taken from Wänke et al. (1984).

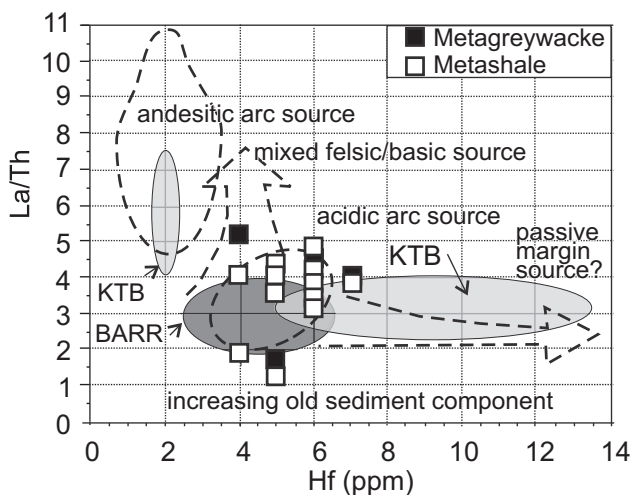


Fig. 7 Metasedimentary rocks of the TCC in the Hf vs. La/Th plot of Floyd and Leveridge (1987).

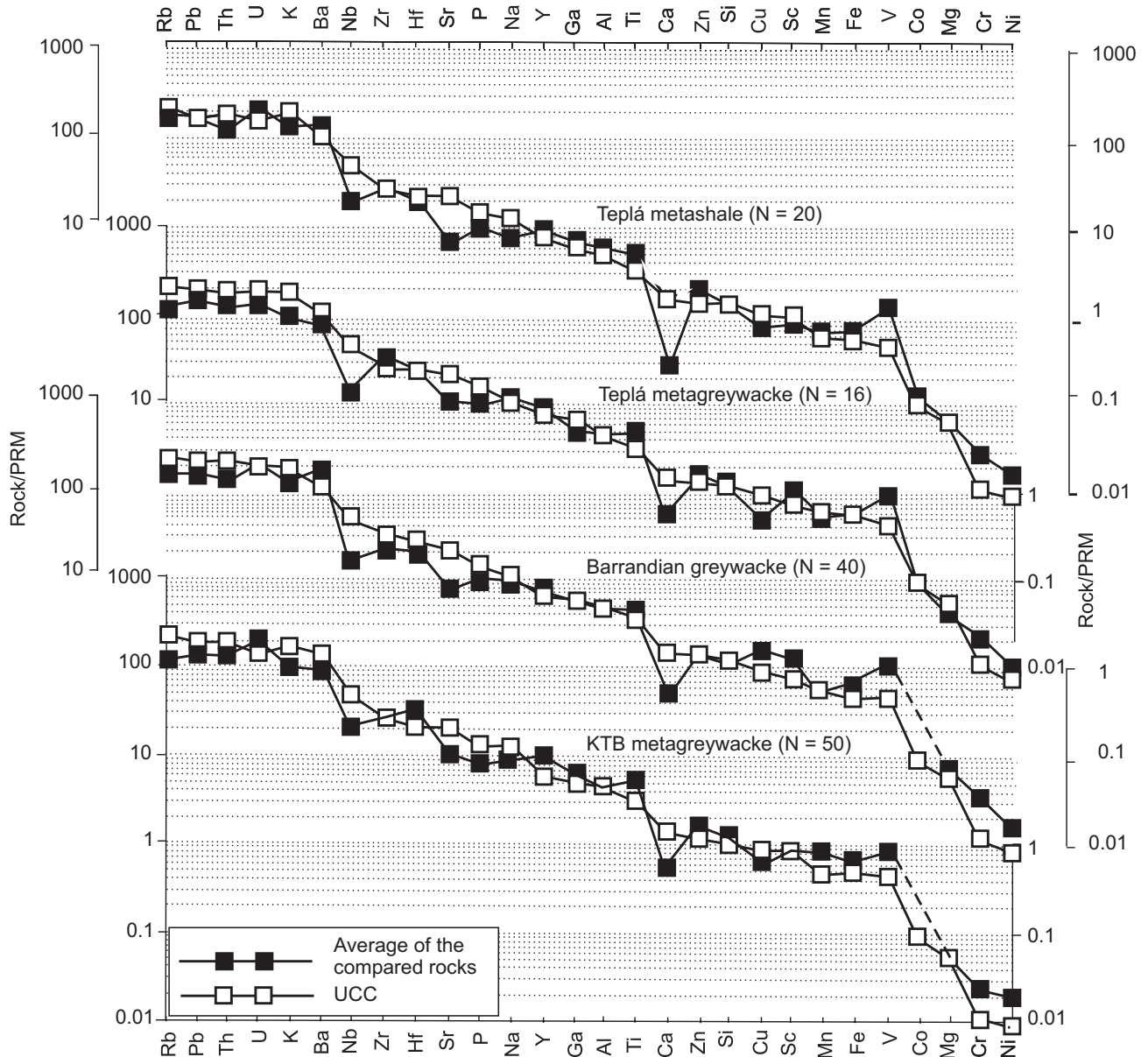


Fig. 8 Multi-element (spider) diagrams of metasedimentary rocks from the Teplá Crystalline Complex and from comparable rocks, all PRM (Primitive Mantle) normalized. Normalization values from Taylor and McLennan (1985). Average Upper Continental Crust (UCC) composition is from Taylor and McLennan (1985) and Wänke et al. (1984).

The PRM-normalized UCC element contents were used as a reference basis for the individual plots.

The TCC data were plotted separately for metashales and metagreywackes to decipher the possible compositional changes due to progressive mechanical and chemical alteration prior to deposition (Fig. 8).

5.4. Rare earth elements (REE)

The REE data of the analysed TCC metasediments are presented in Tab. 4. Chondrite-normalized (Taylor and McLennan 1985) REE patterns can be divided into three groups. The most common pattern (27 samples) is

shown in Fig. 9. This UCC-like distribution is characterized by a steeper course of the LREE, a pronounced negative Eu anomaly ($\text{Eu}/\text{Eu}^* = 0.55\text{--}0.79$) and a rather flat HREE segment. The contents of REE are slightly enhanced relative to the UCC distribution, which holds namely for the HREE. The exception to this overall trend is sample No. 2, wherein the REE content is substantially higher.

Figure 10 presents a less common REE pattern of three TCC samples almost lacking the Eu anomaly, in two cases with a smooth, moderately concave course of distribution. The TCC distribution curves in Fig. 10 are well comparable with those of undifferentiated CIA andesites.

Tab. 4 Rare-earth-element data for the Teplá Crystalline Complex metasediments [ppm]

No.	1	2	3	4	5	6	7	8	9	10	11	12	13	14	15	17	18	19
La	37.9	57.9	33.8	36.5	34.1	31.3	26.6	30.6	31.0	31.8	35.6	30.8	37.0	31.9	33.0	28.5	16.1	11.1
Ce	77.7	119.2	75.5	73.8	103.7	61.6	53.3	70.1	75.6	71.6	70.6	67.0	77.0	76.7	73.0	57.8	58.9	50.6
Pr	8.7	14.6	7.5	9.4	7.4	6.5	5.8	6.4	7.9	7.7	7.0	8.3	8.7	8.1	8.3	7.6	4.4	2.5
Nd	33.0	54.7	31.6	31.6	31.4	27.7	25.3	28.5	28.7	30.4	33.5	30.5	34.7	31.5	31.6	25.6	14.7	11.1
Sm	5.9	11.9	6.2	6.3	6.3	6.2	4.9	5.2	5.4	6.4	7.2	6.3	6.6	5.9	5.8	5.1	4.0	3.0
Eu	1.53	2.18	1.44	1.50	1.58	1.05	1.44	1.34	1.73	1.45	1.59	1.58	1.60	1.40	1.63	0.94	0.75	0.93
Gd	6.7	11.9	5.5	6.9	6.3	4.1	4.9	5.4	5.5	6.0	7.1	5.8	6.6	6.2	6.7	5.2	5.2	4.4
Dy	5.4	10.6	5.8	5.9	5.7	5.6	4.3	5.1	5.7	6.0	5.9	5.7	6.2	5.8	5.9	5.7	6.3	4.5
Ho	1.22	1.83	0.90	1.25	0.92	1.58	0.73	0.92	1.09	0.97	0.76	0.84	1.30	1.02	1.41	2.09	2.00	0.50
Er	3.0	5.7	3.1	3.0	2.7	3.4	2.2	2.8	3.0	2.9	3.6	3.5	3.0	3.0	3.3	3.6	3.8	2.8
Tm	0.47	1.21	0.63	0.56	0.52	0.47	0.18	0.53	0.66	0.49	0.78	0.45	0.77	0.62	0.59	0.56	0.90	0.51
Yb	3.6	6.1	1.8	3.7	3.1	3.2	2.6	2.4	3.1	3.1	3.6	2.8	4.1	3.8	3.7	2.4	3.7	3.6
Lu	0.49	0.84	0.18	0.51	0.41	0.72	0.39	0.28	0.39	0.38	0.47	0.35	0.59	0.49	0.53	0.82	0.87	0.44
Eu/Eu*	0.74	0.55	0.74	0.69	0.76	0.60	0.89	0.77	0.96	0.71	0.67	0.79	0.73	0.71	0.79	0.55	0.50	0.79
Ce/Ce*	0.98	0.94	1.08	0.92	1.48	0.97	0.97	1.13	1.11	1.05	0.99	0.97	0.98	1.10	1.01	0.91	1.62	2.18

No.	20	21	22	23	24	25	26	27	28	29	30	31	32	33	34	35	36	37
La	16.9	11.6	33.2	9.3	36.4	26.4	34.0	36.3	36.8	33.2	31.7	40.6	34.2	26.2	27.2	16.5	36.8	35.2
Ce	50.4	31.0	67.1	22.7	70.9	58.0	70.2	70.5	73.0	67.7	63.6	76.3	72.3	54.7	58.1	51.2	74.8	72.3
Pr	5.1	2.6	9.7	3.1	9.1	6.1	8.0	9.6	9.3	7.1	6.9	8.9	8.1	6.8	7.1	3.1	9.8	9.1
Nd	14.7	10.6	30.8	10.2	34.2	25.9	30.9	33.9	35.1	33.0	26.9	37.0	33.2	26.1	28.2	16.0	37.3	35.2
Sm	3.6	3.2	6.2	2.3	6.6	4.2	6.6	6.6	7.8	6.1	5.2	8.5	6.6	5.6	5.4	4.0	7.2	6.7
Eu	0.89	0.73	1.43	0.62	1.62	1.13	1.35	1.41	1.61	1.53	1.32	1.84	1.52	1.38	1.40	1.01	1.61	1.57
Gd	4.0	3.2	5.8	1.6	6.6	4.7	5.9	6.5	6.7	5.5	6.0	7.9	7.5	4.9	5.4	3.8	6.6	8.1
Dy	4.7	4.6	4.9	3.1	6.0	4.5	5.0	6.5	6.3	5.6	4.8	6.7	5.8	4.4	4.8	4.3	6.5	6.6
Ho	0.92	0.78	0.89	1.02	0.98	0.59	0.94	1.32	1.19	1.07	0.80	1.28	1.24	1.01	0.89	0.75	1.19	1.44
Er	3.0	2.7	2.9	3.0	3.8	2.8	3.0	4.0	3.4	3.5	2.9	4.3	3.4	3.0	3.1	3.1	3.8	4.2
Tm	0.62	0.47	0.58	0.24	0.53	0.58	0.37	0.84	0.84	0.69	0.56	1.06	0.76	0.68	0.56	0.63	1.00	0.72
Yb	3.2	2.2	3.1	2.5	3.3	2.5	2.6	3.8	3.9	3.3	2.8	4.1	3.8	2.7	2.9	3.0	4.1	4.2
Lu	0.38	0.25	0.39	0.53	0.40	0.27	0.32	0.56	0.52	0.44	0.43	0.55	0.51	0.35	0.37	0.38	0.58	0.58
Eu/Eu*	0.71	0.70	0.72	0.95	0.74	0.77	0.65	0.65	0.67	0.79	0.72	0.68	0.66	0.78	0.78	0.78	0.70	0.65
Ce/Ce*	1.26	1.28	0.87	0.99	0.89	1.04	0.97	0.87	0.91	1.00	0.97	0.91	0.99	0.94	0.97	1.58	0.91	0.93

The last REE distribution type is represented by six samples in Fig. 11 which display, besides the negative Eu anomalies, a distinct positive anomaly of Ce; the other LREE are less enriched. These samples from the lower part of the biotite zone (Fig. 1).

5.5. Sr and Nd isotopic studies

From the total of 36 samples for the TCC metasedimentary rocks, nine representative samples were selected for Sr–Nd isotopic studies. Four samples from anchi- to unmetamorphosed Barrandian sedimentary rocks were also selected for comparison (“K-” samples from the geochemical database of Czech Geological Survey, Čadková et al. 1985). The resulting data are presented in Tab. 5.

The sedimentation age of 550 Ma used for calculation of Sr initial ratios and epsilon Nd values is constrained by the existing zircon U–Pb data for the Teplá orthogneiss, which are interpreted as dating emplacement of its protolith (Dörr et al. 1995). The application of single- and two-stage evolution models of the Sm–Nd system

(DePaolo 1991) yielded two groups of T_{DM} model ages. The difference of T_{DM} values between the two models is mostly negligible except for samples with a positive Ce anomaly. The latter yielded generally higher model ages ($T_{DM-single} = 1.8–2.0$ Ga) than the other samples ($T_{DM} = 1.0–1.5$ Ga). The initial $^{87}Sr/^{86}Sr$ ratios for all samples are fairly constant and compatible with the assumption of a dominance of detrital material, that was isotopically less evolved.

Figure 12 represents the $^{87}Sr/^{86}Sr(T)$ vs. $\epsilon_{Nd}(T)$ plot for the TCC and ZEV (including KTB) metasedimentary rocks. Variation fields of some Saxothuringian and Moldanubian metasediments are given for comparison (Liew and Hofmann 1988; Henjes-Kunst 2000). The KTB data (KTB–VB) come also from von Drach and Köhler (1993). In general, two groups of data are observed: one containing TCC, ZEV, KTB–VB and unmetamorphosed Barrandian (BARR), and another one of Saxothuringian and Moldanubian samples. Plots $La_N/Yb_N - \epsilon_{Nd}(T)$ and $^{87}Sr/^{86}Sr(T) - \epsilon_{Nd}(T)$ (Fig. 13) illustrates the Sr–Nd isotopic evolution of the Barrandian (meta-) sedimentary rocks in time.

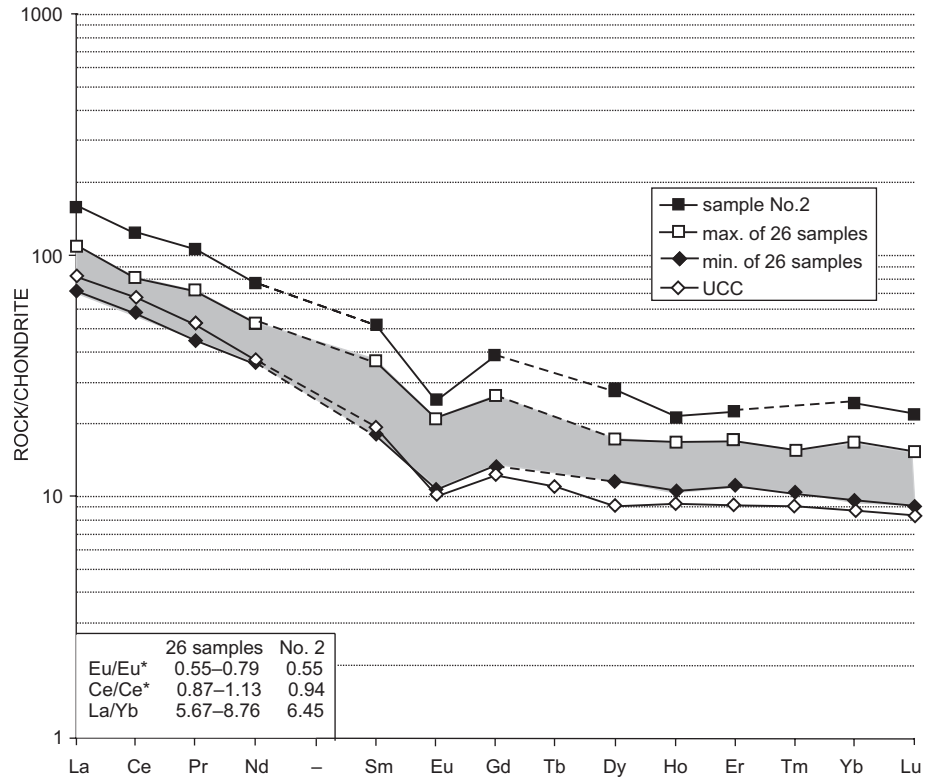


Fig. 9 Chondrite-normalized (Taylor and McLennan 1985) REE distribution in 27 metasedimentary rocks of the Teplá Crystalline Complex (Nos. 1-4, 6, 8, 10-15, 17, 22, 24-34, 36, 37). For UCC composition, see Fig. 7.

6. Discussion

The multielement distribution curves on the Fig. 8 display several distinct anomalies connected predominantly to the character of the source rocks and the subsequent disintegration and weathering processes. Comparison of sedimentologically primitive greywackes with more mature shales shows mostly an increase in positive anomalies and a decrease in negative anomalies with the increasing maturity of sediments. The only exceptions are negative anomalies of Ca and Sr, which deepen in more mature sediments. This can be explained by synergy of two processes: mechanical disintegration, which elevated the trace element-rich pelitic component in shales, and progressive chemical decomposition

of plagioclase, leading to liberation of part of the Ca and Sr into seawater.

The differences from the reference UCC curve will be discussed for the TCC metagreywackes because

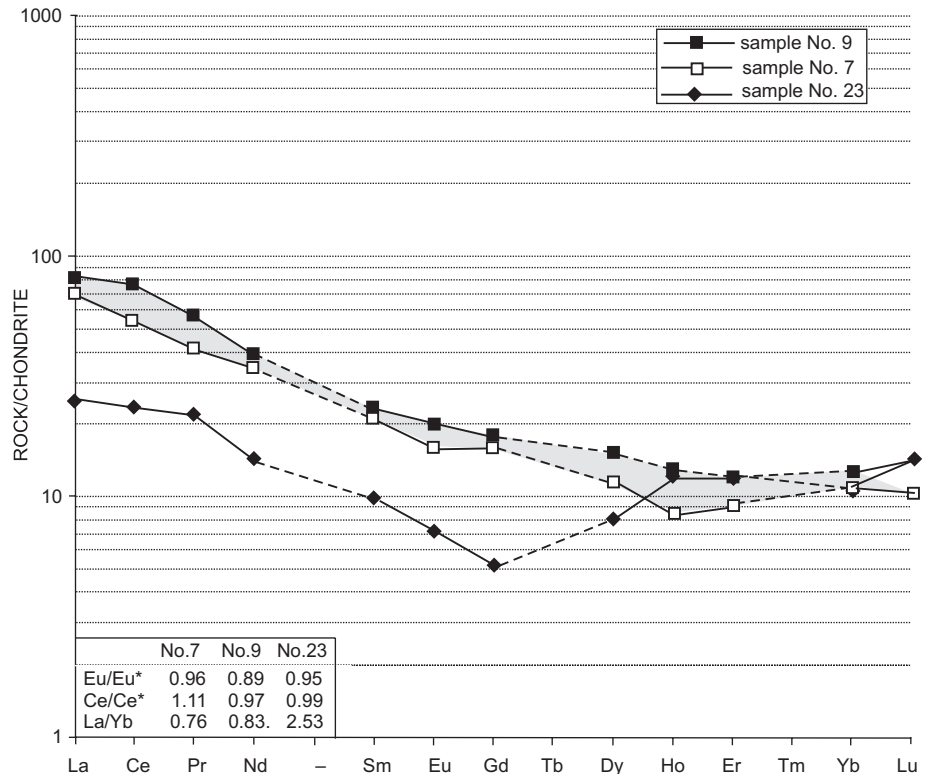


Fig. 10 Chondrite-normalized (Taylor and McLennan 1985) REE distribution in three metasedimentary rocks of the Teplá Crystalline Complex.

Tab. 5 Sr–Nd isotopic composition of metasediments of the Teplá Crystalline Complex, measured and calculated data, age-corrected to T = 550 Ma

No.	Variety	Locality	Rb [ppm]	Sr [ppm]	⁸⁷ Rb/ ⁸⁶ Sr	Sm [ppm]	Nd [ppm]	¹⁴⁷ Sm/ ¹⁴⁴ Nd	¹⁴³ Nd/ ¹⁴⁴ Nd	Note	Rb/Sr	⁸⁷ Sr/ ⁸⁶ Sr(T)	Sm/Nd	¹⁴⁸ Nd/ ¹⁴⁴ Nd(T)	$\epsilon_{Nd}(0)$	$\epsilon_{Nd}(T)$	$\frac{^{147}\text{Sm}}{^{144}\text{Nd}} \text{ [Ga]}$	$\frac{^{147}\text{Sm}}{^{144}\text{Nd}} \text{ (T)}$	$\frac{^{147}\text{Sm}}{^{144}\text{Nd}} \text{ (2-st)}$
1	shl	Kojšovice	86	122	1.945	0.72404	5.9	33.0	0.1194	0.512261	0.7049	0.7088	0.1788	0.511831	-7.35	-1.92	1.36	1.40	
8	grw	Dobrá Voda	68	127	1.620	0.71976	5.2	28.5	0.1212	0.512352	0.5354	0.7071	0.1825	0.511915	-5.58	-0.27	1.24	1.26	
9	grw	Braníšov	68	204	0.992	0.71637	5.4	28.7	0.1228	0.512439	0.3333	0.7086	0.1882	0.511996	-3.88	1.31	1.13	1.13	
11	shl	Vidžín	96	148	2.002	0.72215	7.2	33.5	0.1219	0.512333	0.6486	0.7065	0.2149	0.511894	-5.95	-0.69	1.28	1.30	
17	grw	Krsy	66	223	0.907	0.71241	5.1	25.6	0.1262	0.512490	0.2960	0.7053	0.1992	0.512035	-2.89	2.07	1.09	1.06	
18	shl	Ostrov	89	120	1.933	0.72376	4.0	14.7	0.1456	0.512285	0.7417	0.7087	0.2721	0.511760	-6.89	-3.30	1.79	1.50	
19	grw	Ostrov	64	122	1.621	0.71880	3.0	11.1	0.1515	0.512266	0.5246	0.7061	0.2703	0.511720	-7.26	-4.08	1.99	1.56	
21	shl	Starý Mlýn	104	99	3.118	0.72798	3.2	10.6	0.1416	0.512251	1.0505	0.7036	0.3019	0.511741	-7.55	-3.68	1.77	1.53	
27	shl	Rabštejn	93	89	3.141	0.72958	6.6	33.9	0.1215	0.512207	1.0449	0.7050	0.1947	0.511769	-8.41	-3.13	1.47	1.49	
K-37	grw	Všehrdy	58	80	1.811	0.71806	5.28	25.92	0.1227	0.512544	0.7250	0.7039	0.2037	0.512102	-1.83	3.37	0.96	0.95	
K-60	grw	Hluboká	30	172	1.028	0.71277	3.88	17.97	0.1299	0.512304	0.1744	0.7078	0.2159	0.511836	-6.52	-1.82	1.45	1.39	
K-62	grw	Těchlovice	45	173	0.633	0.71214	3.90	18.54	0.1266	0.512481	0.2601	0.7049	0.2104	0.512025	-3.06	1.87	1.10	1.08	
K-74	grw	Hromnice	56	178	0.928	0.71212	5.86	27.86	0.1267	0.512521	0.3146	0.7041	0.2103	0.512064	-2.28	2.64	1.04	1.01	

Constants used for calculations: $\lambda_{Rb} = 0.0139 \text{ } \text{A}^{-1}$, $\frac{^{87}\text{Sr}}{^{86}\text{Sr}}_{\text{UR}}(0) = 0.7045$, $\frac{^{87}\text{Rb}}{^{86}\text{Sr}}_{\text{UR}}(0) = 0.0839$, $\lambda_{Sm} = 0.00654 \text{ } \text{A}^{-1}$, $\frac{^{143}\text{Nd}}{^{144}\text{Nd}}_{\text{CHUR}}(0) = 0.512638$, $\frac{^{147}\text{Sm}}{^{144}\text{Nd}}_{\text{CHUR}}(0) = 0.1967$, $1 \text{ } \text{A} = 10^9 \text{ a}$ (Steiger and Jäger 1977, Jacobsen and Wasserburg 1980)

they reflect the primary composition better than the metashales. Large ion lithophile elements (LILE) from Rb to Ba in the TCC metagreywackes show a marked depletion relative to UCC, which documents their immature character from the crustal evolution point of view. The conspicuous negative Nb anomaly leads to the same conclusion, as it is usually explained (e.g., Bonjour and Dabard 1991; Slack and Stevens 1994) by the absence of the Nb-rich anorogenic granites in the immature crust. The positive anomalies of Ti, Sc, V, Mg, Cr and Ni are indicative of variable mafic input from oceanic intraplate environment. The slight positive or negative “heavy mineral” anomalies of Zr, Hf and Y probably point to sedimentary processes, such as density sorting during transport. The above-mentioned characteristics are compatible with a prevailing continental island-arc source with a smaller variable admixture of oceanic mafic rocks and limited continental detrital material (e.g., Floyd et al. 1991). The problem of residual negative Ca and Sr anomalies remaining conspicuous even in the supposedly chemically little altered metagreywackes is still open. Jakeš et al. (1979) supposed an input of the spilitised basic volcanic detritus to solve the depletion in Sr in the Barandian greywackes. The behavior of Cu is ambiguous and could be connected with depletions or enrichments due to mineralization processes.

A comparison of elemental distributions between the metamorphosed (TCC, KTB) and unmetamorphosed (BARR) greywackes does not reveal any substantial changes due to regional metamorphism. Moreover, similar distribution patterns of the TCC, BARR and KTB data suggest close genetic relations of the studied rocks from the mentioned units.

The REE distribution curves of the TCC samples form three principal groups. The major group of 26 samples (Fig. 9) displays pronounced negative Eu anomalies. According to McLennan et al. (1993), the negative Eu anomaly suggests that igneous rocks of the continental-island arc provenance were formed by intra-crustal plagioclase fractionation. A comparison with the REE patterns of modern deep-sea turbidites (McLennan and Taylor 1991) shows a close similarity with those of continental island arcs.

The second group (Fig. 10) contains three samples and is without any Eu anomaly. Such pattern exists in andesites of both the continental and the oceanic-island arcs. The difference consists in a higher REE content and a steeper course of the distribution curve of CIA andesites compared to OIA settings (cf. Bhatia 1985; McLennan and Taylor 1991). This variation in REE patterns of CIA andesites depends on the degree of crystal differentiation during magma ascent, which is enhanced within the continental settings.

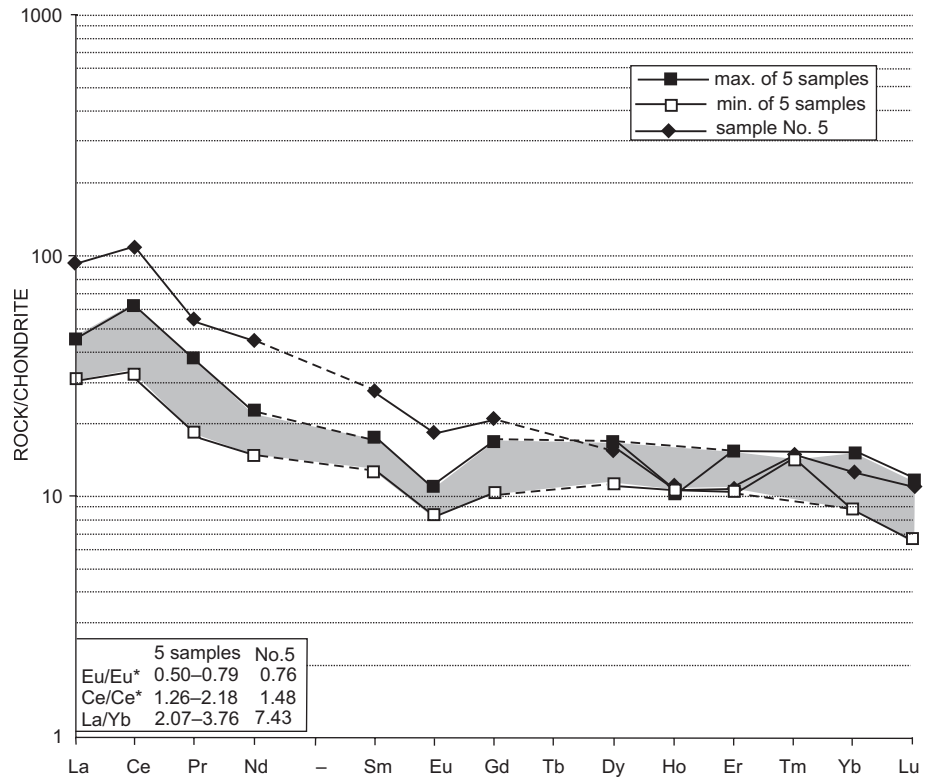


Fig 11 Chondrite-normalized (Taylor and McLennan 1985) REE distribution in six metasedimentary rocks of the Teplá Crystalline Complex displaying positive Ce anomalies.

The third group containing six samples (Fig. 11) displays, besides Eu negative anomalies, also a distinct anomaly of Ce. This feature can be attributed to LREE leaching during sedimentation under oxidizing conditions, whereby Ce^{4+} remains in the sediment (McDaniel et al. 1994).

Results of the Rb–Sr and Sm–Nd isotopic analyses presented in Fig. 12 distinguish two groups of geological units in the Bohemian Massif in the $\epsilon_{Nd}(T)$ vs. $^{87}Sr/^{86}Sr(T)$ plot. The first group containing TCC, KTB–VB, ZEV and Barranian displays $\epsilon_{Nd}(T)$ values between –4 and +4, the second one, containing Moldanubian and Saxothuringian samples,

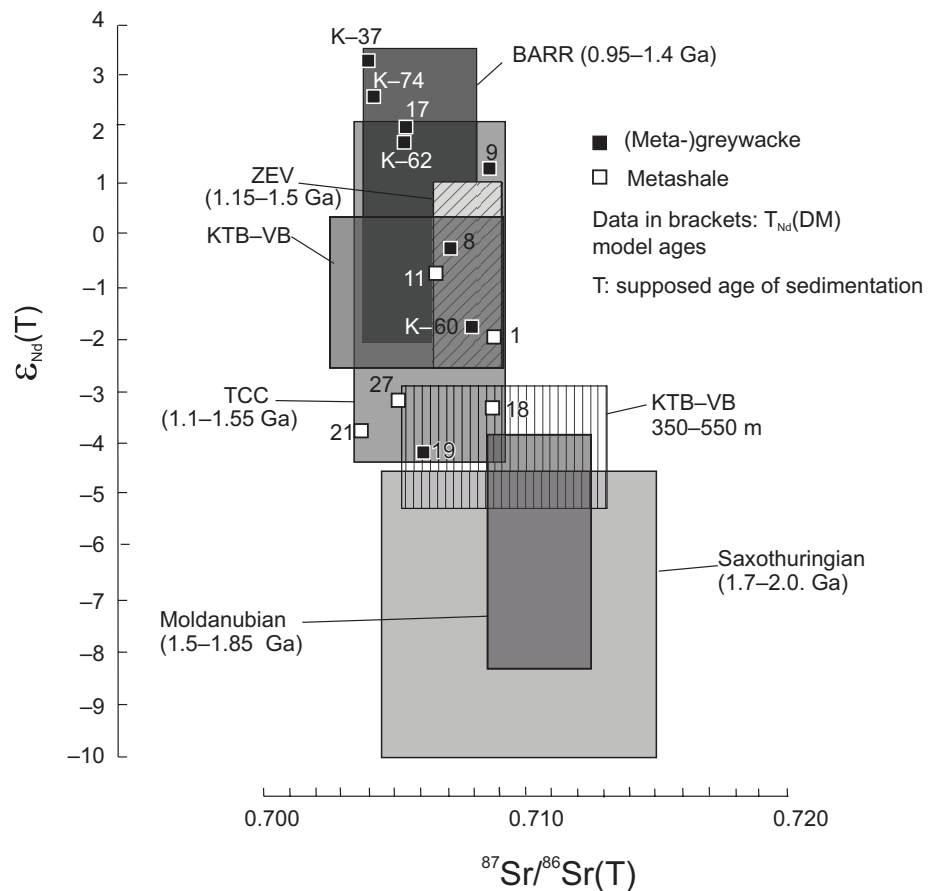


Fig. 12 Variation fields in $^{87}Sr/^{86}Sr(T)$ vs. $\epsilon_{Nd}(T)$ binary plot for the Teplá Crystalline Complex and for comparable units. Data sources: this work, Liew and Hofmann (1988) von Drach and Köhler (1993) and Henjes-Kunst (2000).

Tab. 6 Comparison of TCC metasediments and accretionary wedge sediments from Kamchatka (Russia), according Ledneva et al. (2004)

	N	K ₂ O/Al ₂ O ₃	(Fe ₂ O ₃ +MgO)/SiO ₂	Al ₂ O ₃ /SiO ₂	CIA	Fe/Mn	(La/Yb) _N	Eu/Eu*	Ce/Ce*	Th/U	Th/Sc	La/Sc	Rb/Sr	Cr/Ni
Teplá	36	0.15	0.12	0.25	65.12	63.17	6.55	0.66	1.00	3.12	0.58	2.17	0.60	3.53
Kamchatka	18	0.14	0.15	0.24	67.53	48.69	6.73	0.67	0.96	2.97	0.40	1.31	0.53	2.55

falls within the interval of -4 to -10 . This difference evidently reflects the prevalence of rather juvenile material in the first group and, on the other hand, the prevalence of old evolved crustal material in the second one. This is supported by the lower model ages T_{Nd} (DM) = 0.95 – 1.5 Ga of the former group compared to those of the latter one (1.5 – 2.0 Ga). Combining our data with those of Drost et al. (2007), we can follow on the Fig. 13 the gradual increase of the evolved continental crust component with the decreasing age of sediments. Our “K-” samples of unmetamorphosed Neoproterozoic greywackes represent the most primitive material of the whole Teplá–Barrandian sample set. Connecting the Rb–Sr systematics, all our samples plot outside the shaded zone; this indicates that no substantial late Rb-gain or Sr-loss occurred.

Our results of geochemical and isotopic investigations of the TCC metasediments point to their continental island-arc provenance. Štědrá et al. (2002) discussed two possible scenarios for geotectonic setting of the TCC: (1) a deeply reworked part of an accretionary wedge at a Gondwana margin, and (2) a subducted segment of an active continental margin with incorporated back-arc slivers and metasedimentary and magmatic oceanic rocks. The hypothesis #1 is (together with Zulauf 1997 and Dörr et al. 2002) one of the first suggestions of the accretionary wedge provenance in the Teplá–Barrandian. The results of geochemical and isotopic studies of Barrandian metabasalts (Pin and Waldhausrová 2007) sup-

port this idea, further elaborated by Hajná et al. (2010) in the central and NW parts of this unit. In the current paper, we have attempted to evaluate this hypothesis using new geochemical data. The principal question, however, is to what degree can the two environments (i.e., the continental-island arc and the accretionary wedge) be unequivocally distinguished on the basis of difference in the geochemistry of sedimentary rocks.

To address this issue, we compare our results with a modern example of accretionary wedge sediments from Russian Kamchatka. There, a detailed geochemical study of Ledneva et al. (2004) documented the nature of the NE Asian active continental margin in the middle Eocene to early Miocene. The trace-element geochemistry of shales from the flysch and mélangé indicates the derivation of this sediment types from an active continental margin and island arcs with partially dissected basement rocks. Such provenance characteristics are similar to those of the continental-island arc and, therefore, we can hardly expect any significant geochemical features to distinguish between the two geotectonic settings. The comparison of the TCC and the Kamchatka accretionary wedge points to their similar lithology (mostly flysch-like sediments and mélangé). Regarding the principal geochemical features (some summarized in Tab. 6), the striking similarities include, e.g., the high LREE abundance, pronounced negative Eu anomaly, low Th/Sc and La/Sc ratios, negative Nb anomaly in relation to average upper crust etc. Small differences in some of the ratios can be explained

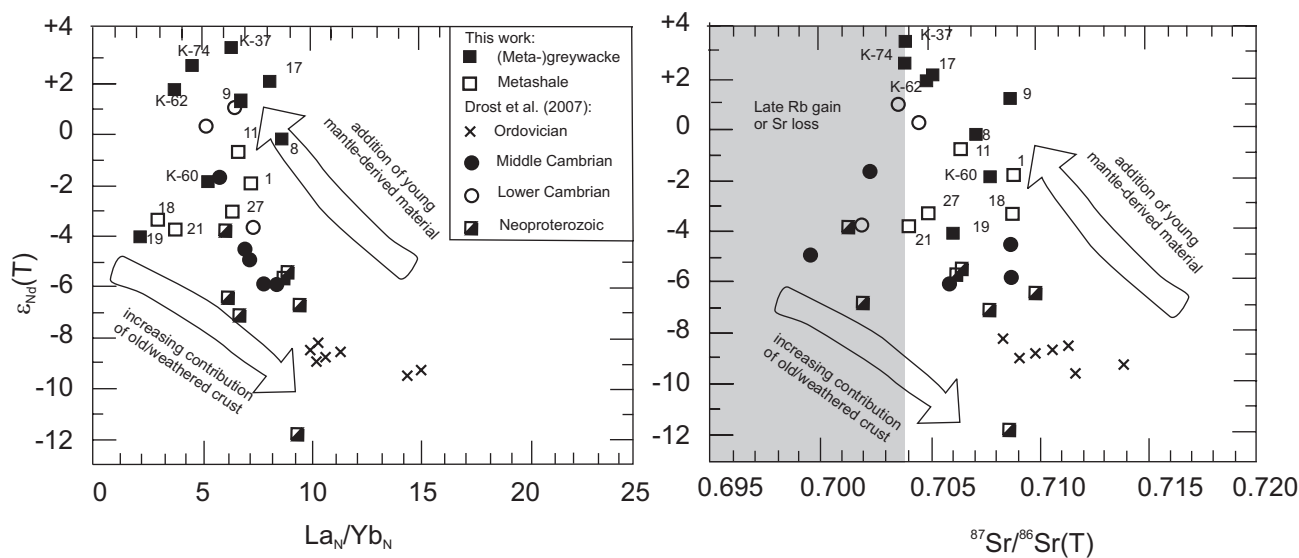


Fig. 13 Metasedimentary rocks of the Teplá Crystalline Complex in the binary diagram of Drost et al. (2007) involving Nd isotopic compositions. **a** – La_N/Yb_N vs. $\epsilon_{Nd}(T)$; Chondrite normalization after Taylor and McLennan (1985). **b** – $^{87}Sr/^{86}Sr(T)$ vs. $\epsilon_{Nd}(T)$ plot.

by local variations, e.g., deep- or shallow-water conditions (Fe/Mn) and various admixtures of volcanic vs. ultramafic sources (Cr/Ni).

7. Conclusions

An extensive geochemical and Sr–Nd isotopic investigation of the Teplá Crystalline Complex clastic metasedimentary rocks revealed their active continental margin affinity with an important role of underlying or nearby situated continental crust. Pure geochemical and isotopic criteria point to a relatively immature continental (ensialic) island arc. A comparison with the Tertiary accretionary wedge sedimentary complex (Kamchatka/Russia) shows striking geochemical similarities. The accretionary wedge idea is therefore consistent with a continental-arc provenance as derived from the rock geochemistry. The tectonic arguments and incompatibility of the Teplá–Barrandian metabasalts with their (meta-) sedimentary host represent further important constraints for the acceptance of the accretionary wedge provenance hypothesis for parts of the Neoproterozoic to early Cambrian sedimentary complexes of the Teplá–Barrandian Unit.

Acknowledgements. We are indebted to the Institute of Geology ASCR internal grant No. 9334 for the financial support to finishing this work. We also acknowledge the both anonymous reviewers for the critical useful comments and namely editors V. Janoušek and J. Žák for substantial improvement of the present paper. We are obliged to J. Adamovič for kind revision of English.

References

- BEARD BL, MEDARIS JR LG, JOHNSON CM, JELÍNEK E, TONIKA J, RICIPUTI LR (1995) Geochronology and geochemistry of eclogites from the Mariánské Lázně Complex, Czech Republic: implications for Variscan orogenesis. *Geol Rundsch* 84: 552–567
- BHATIA MR (1983) Plate tectonics and geochemical composition of sandstones. *J Geol* 91: 611–627
- BHATIA MR (1985) Rare earth element geochemistry of Australian Paleozoic graywackes and mudrocks: provenance and tectonic control. *Sediment Geol* 45: 97–113
- BHATIA MR, CROOK KAW (1986) Trace element characteristics of graywackes and tectonic setting of sedimentary basins. *Contrib Mineral Petrol* 92: 181–193
- BONJOUR JL, DABARD MP (1991) Ti/Nb ratios of clastic terrigenous sediments used as an indicator of provenance. *Chem Geol* 91: 257–267
- BOWES DR, AFTALION M (1991) U–Pb zircon isotopic evidence for early Ordovician and late Proterozoic units in the Mariánské Lázně Complex, Central European Hercynides. *Neu Jb Mineral, Mh* 7: 315–326
- CERRAI E, TESTA C (1963) Separation of rare earths by means of small columns of Kel–F supporting di(2-ethylhexyl) orthophosphoric acid. *J Inorg Nucl Chem* 25: 1045–1050
- ČADKOVÁ Z, MRÁZEK P (1987) Trends of trace element distribution in several selected lithostratigraphic units of the Bohemian Massif. *Čas Mineral Geol* 32: 371–392 (in Czech with English summary)
- ČADKOVÁ Z, JAKEŠ P, HAKOVÁ M, MRÁZEK P (1985) Geochemical catalogue of the basic network. Unpublished database, Czech Geological Survey, Prague (in Czech)
- CHÁB J (1978) Proposals of the lithostratigraphic and lithologic terminology for the Upper Proterozoic of the Teplá–Barrandian region. *Věst Ústř Úst geol* 53: 43–60 (in Czech)
- CHÁB J, PELC Z (1968) Lithology of Upper Proterozoic in the NW limb of the Barrandian area. *Krystalinikum* 6: 141–167
- CHÁB J, PELC Z (1973) Proterozoische Grauwacken im NW–Teil des Barrandiums (Tschechisch). *Sbor geol Věd* 25: 7–84
- CHÁB J, ŽÁČEK V (1994) Metamorphism of the Teplá Crystalline Complex. *KTB Report 94-3*: 33–37
- DALLMEYER RD, URBAN M (1998) Variscan vs. Cadomian tectonothermal activity in the northwestern sectors of the Teplá–Barrandian zone, Czech Republic: constraints from ⁴⁰Ar/³⁹Ar ages. *Geol Rundsch* 87: 94–106
- DEPAOLO DJ, LINN AM, SCHUBERT G (1991) The continental crustal age distribution: methods of determining mantle separation ages from Sm–Nd isotopic data and application to the southwestern United States. *J Geophys Res* 96 B2: 2071–2088
- DÖRR W, FIALA J, PHILLIPE S, VEJNAR Z, ZULAUF G (1995) Cadomian vs. Variscan imprints in the Teplá–Barrandian Unit. – Part A: U–Pb ages of pre-Variscan granitoids. *Terra Nostra* 95: 91–92
- DÖRR W, FIALA J, VEJNAR Z, ZULAUF G (1998) U–Pb zircon ages and structural development of metagranitoids of the Teplá Crystalline Complex: evidence for pervasive Cambrian plutonism within the Bohemian Massif (Czech Republic) *Geol Rundsch* 87: 135–149
- DÖRR W, ZULAUF G, FIALA J, FRANKE W, VEJNAR Z (2002) Neoproterozoic to Early Cambrian history of an active plate margin in the Teplá–Barrandian Unit – a correlation of U–Pb isotopic-dilution-TIMS ages (Bohemia, Czech Republic). *Tectonophysics* 352: 65–85
- DROST K, LINNEMANN U, MCNAUGHTON N, FATKA O, KRAFT P, GEHMLICH M, TONK CH, MAREK J (2004) New data on the Neoproterozoic–Cambrian geotectonic setting of the Teplá–Barrandian volcano-sedimentary successions: geochemistry, U–Pb zircon ages, and provenance (Bohemian Massif, Czech Republic). *Int J Earth Sci* 93: 742–757
- DROST K, ROMER RL, LINNEMANN U, FATKA O, KRAFT P, MAREK J (2007) Nd–Sr–Pb isotopic signatures of Neopro-

- terozoic–Early Paleozoic siliciclastic rocks in response to changing geotectonic regimes: a case study from the Barrandian area (Bohemian Massif, Czech Republic). In: LINNEMANN U, NANCE RD, KRAFT P, ZULAUF G (eds) *The Evolution of the Rheic Ocean: From Avalonian–Cadomian Active Margin to Alleghenian–Variscan Collision*. Geological Society of America Special Papers 423: 191–208
- FLOYD PA, LEVERIDGE BE (1987) Tectonic environment of the Devonian Gramscatho Basin, south Cornwall: framework mode and geochemical evidence from turbiditic sandstones. *J Geol Soc, London* 141: 531–542
- FLOYD PA, SHAIL R, LEVERIDGE BE, FRANKE W (1991) Geochemistry and provenance of Rhenohercynian synorogenic sandstones: implications for tectonic environment discrimination. In: MORTON AC, TODD SP, HAUGHTON PDW (eds) *Developments in Sedimentary Provenance Studies*. Geological Society London Special Publications 57: 173–188
- GLODNY J, GRAUERT B, FIALA J, VEJNAR Z, KROHE A (1998) Metapegmatites in the western Bohemian Massif: ages of crystallisation and metamorphic overprint, as constrained by U–Pb zircon, monazite, garnet, columbite and Rb–Sr muscovite data. *Geol Rundsch* 87: 124–134
- HAJNÁ J, ŽÁK J, KACHLÍK V, CHADIMA M (2010) Subduction-driven shortening and differential exhumation in a Cadomian accretionary wedge: the Teplá–Barrandian Unit, Bohemian Massif. *Precambrian Res* 176: 27–45
- HAJNÁ J, ŽÁK J, KACHLÍK V (2011) Structure and stratigraphy of the Teplá–Barrandian Neoproterozoic, Bohemian Massif: a new plate-tectonic reinterpretation. *Gondwana Res* 19: 495–508
- HAJNÁ J, ŽÁK J, KACHLÍK V, CHADIMA M (2012) Deciphering the Variscan tectonothermal overprint and deformation partitioning in the Cadomian basement of the Teplá–Barrandian Unit, Bohemian Massif. *Int J Earth Sci (Geol Rundsch)* 101: 1855–1873
- HAJNÁ J, ŽÁK J, KACHLÍK V, DÖRR W, GERDES A (2013) Neoproterozoic to early Cambrian Franciscan-type mélanges in the Teplá–Barrandian Unit, Bohemian Massif: evidence of modern-style accretionary processes along the Cadomian active margin of Gondwana? *Precambrian Res* 224: 653–670
- HENJES-KUNST F (2000) *Isotopie. Abschlussbericht Mu 897/4 DFG-SPP “Orogene Prozesse” – Teil 4: 1–4*. Unpublished report, BGR Hannover
- HOLUBEC J (1966) Stratigraphy of the Upper Proterozoic in the core of the Bohemian Massif (Teplá–Barrandian region). *Rozpr Čs Akad Věd, Ř mat příř Věd* 76: 1–62
- JACOBSEN SB, WASSERBURG GJ (1980) Sm–Nd isotopic evolution of chondrites. *Earth Planet Sci Lett* 50: 139–155
- JAKEŠ P, ZOUBEK J, ZOUBKOVÁ J, FRANKE W (1979) Graywackes and metagraywackes of the Teplá–Barrandian Proterozoic area. *Sbor geol Věd, Geol* 33: 83–122
- KACHLÍK V (1993) The evidence for Late Variscan nappe thrusting of the Mariánské Lázně Complex over the Saxothuringian terrane (W. Bohemia). *J Czech Geol Soc* 38: 46–58
- KACHLÍK V (1994) The Kladská Unit – petrological and structural evidence for Variscan thrusting of the Mariánské Lázně Complex over the Saxothuringian Terrane (West Bohemia). *KTB Report 94-3: 19–31*
- KETTNER R (1917) Versuch einer stratigraphischen Einteilung des Böhmisches Algonkiums. *Geol Rundsch* 8: 169–188
- KOŠLER J, BOWES DR, FARROW CM, HOPGOOD AM, RIEDER M, ROGERS G (1997) Constraints on the timing of events in the multiepisodic history of the Teplá–Barrandian Complex, western Bohemia, from integration of deformational sequence and Rb–Sr isotopic data. *Neu Jb Mineral, Mh* 1997: 203–220
- KRATOCHVÍL F, VACHTL J, ZOUBEK V (1951) Geological relationships of the Kříženeč–Nezdice Belt of the Teplá Upland. *Sb Ústř Úst geol XVIII: 201–232* (in Czech)
- KRETZ R (1983) Symbols for rock-forming minerals. *Amer Miner* 68: 277–279
- KREUZER H, VEJNAR Z, SCHÜSSLER U, OKRUSCH M, SEIDEL E (1992) K–Ar dating in the Teplá–Domažlice Zone at the western margin of the Bohemian Massif. In: KUKAL Z (ed.) *Proceedings of the 1st International Conference on the Bohemian Massif*. Czech Geological Survey, Prague, pp 168–175
- KŘÍBEK B, POUBA Z, SKOČEK V, WALDHAUSROVÁ J (2000) Neoproterozoic of the Teplá–Barrandian Unit as a part of the Cadomian orogenic belt: a review and correlation aspects. *Bull Geosci* 75: 175–196
- LANG M (2000) Composition of Proterozoic greywackes in the Barrandian. *Bull Geosci* 75: 205–216
- LEDNEVA GV, GARVER JI, SHAPIRO MN, LEDERER J, BRANDON MT, HOLLOCHER KT (2004) Provenance and tectonic settings of accretionary wedge sediments on northeastern Karaginski Island (Kamchatka, Russian Far East). *Russian J Earth Sci* 6: 105–132
- LIEW TC, HOFMANN AW (1988) Precambrian crustal components, plutonic associations, plate environment of the Hercynian Fold Belt of central Europe: indications from a Nd and Sr isotopic study. *Contrib Mineral Petrol* 98: 129–138
- MAŠEK J (2000) Stratigraphy of the Proterozoic of the Barrandian area. *Bull Geosci* 75: 197–200
- MAŠEK J, ZOUBEK J (1980) Proposal of stratigraphical terms for stratigraphical units of the Barrandian Proterozoic. *Věst Ústř Úst geol* 55: 121–123 (in Czech)
- MATĚJKA D (1988) Geochemistry of Upper Proterozoic rocks of the Svojšín volcanic strip (Western Bohemia) and problem of the source material of metasediments. *Geol Carpath* 39: 109–122
- MATTE P, MALUSKI H, RAJLICH P, FRANKE W (1990) Terrane boundaries in the Bohemian Massif: result of large-scale Variscan shearing. *Tectonophysics* 177: 151–170

- MCDANIEL D, HEMMING S, McLENNAN S, HANSON G (1994) Resetting of neodymium isotopes and redistribution of REEs during sedimentary processes: the Early Proterozoic Chelmsford Formation, Sudbury Basin, Ontario, Canada. *Geochim Cosmochim Acta* 58: 931–941
- McLENNAN SM, TAYLOR SR (1991) Sedimentary rocks and crustal evolution: tectonic setting and secular trends. *J Geol* 99: 1–21
- McLENNAN SM, HEMMING S, MCDANIEL DK, HANSON GN (1993) Geochemical approaches to sedimentation, provenances and tectonics. In: JOHNSSON MJ, BASU A (eds) *Processes Controlling the Composition of Clastic Sediments*. Geological Society of America Special Papers 284: 21–40
- MRÁZEK P (1984) Minor and trace elements in rocks of the Bohemian Upper Proterozoic. *Sbor geol Věd, ložisk Geol Mineral* 26: 81–104 (in Czech with English summary)
- MÜLLER H (1989) Geochemistry of metasediments in the Hercynian and pre-Hercynian crust of the Schwarzwald, the Vosges and Northern Switzerland. *Tectonophysics* 157: 97–108
- NESBITT HW, YOUNG GM (1982) Early Proterozoic climate and plate motions inferred from major element chemistry of lutites. *Nature* 299: 715–717
- NORRISH K, CHAPPELL BW (1977) X-ray Fluorescence Spectrometry. In: ZUSSMAN J (ed) *Physical Methods in Determinative Mineralogy*, 2nd edition. Academic Press, London, pp 201–272
- PIN C, WALDHAUSROVÁ J (2007) Sm–Nd isotope and trace element study of Late Proterozoic metabasalts (“spilites”) from the Central Barrandian domain (Bohemian Massif, Czech Republic). In: LINNEMANN U, NANCE RD, KRAFT P, ZULAUF G (eds) *The Evolution of the Rheic Ocean: From Avalonian–Cadomian Active Margin to Alleghenian–Variscan Collision*. Geological Society of America Special Papers 423: 231–247
- POVONDRA P, ŠULCEK Z, DOLEŽAL J (1968) Decomposition Techniques in Inorganic Analysis. Elsevier, Amsterdam, pp 1–224
- RÖHLICH P (1965) Geologische Probleme des mittelböhmisches Alpinkiums. *Geologie* 14.4: 373–403
- RÖHLICH P (2000) Some stratigraphic problems of the Barrandian Neoproterozoic. *Bull Geosci* 75: 201–204
- SLACK JF, STEVENS PJ (1994) Clastic metasediments of the Early Proterozoic Broken Hill Group, New South Wales, Australia: geochemistry, provenance, and metallogenic significance. *Geochim Cosmochim Acta* 58: 3633–3652
- ŠTĚDRÁ V, KACHLÍK V, KRYZA R (2002) Coronitic metagabbros of the Mariánské Lázně Complex and Teplá Crystalline Unit: inferences for the tectonometamorphic evolution of the western margin of the Teplá–Barrandian Unit, Bohemian Massif. In: WINCHESTER JA, PHARAOH TC, VERNIERS J (eds) *Palaeozoic Amalgamation of Central Europe*. Geological Society London Special Publications 201: 217–236
- STEIGER RH, JÄGER E (1977) Subcommission on geochronology: convention on the use of decay constants in geo- and cosmochronology. *Earth Planet Sci Lett* 36: 359–362
- TAYLOR SR, McLENNAN SM (1985) *The Continental Crust: Its Composition and Evolution*. Oxford, Blackwell, pp 1–312
- TIMMERMANN H, ŠTĚDRÁ V, GERDES A, NOBLE SR, PARRISH RR, DÖRR W (2004) The problem of dating high-pressure metamorphism: a U–Pb isotope and geochemical study on eclogites and related rocks of the Mariánské Lázně Complex, Czech Republic. *J Petrol* 45: 1311–1338
- TIMMERMANN H, DÖRR W, KRENN E, FINGER F, ZULAUF G (2006) Conventional and in situ geochronology of the Teplá Crystalline unit, Bohemian Massif: implications for the processes involving monazite formation. *Int J Earth Sci (Geol Rundsch)* 95: 629–647
- VEJNAR Z, ZOUBEK V (1962) Explanations to Geological Map of the ČSSR 1 : 200 000, sheets M-33-XIX Mariánské Lázně and M-33-XXV Švarcava. Czech Geological Survey, Prague (in Czech)
- VON DRACH V, KÖHLER H (1993) Geochronologisches Profil der KTB-Vorbohrung. *KTB-Report* 93-2: 385–388
- WÄNKE H, DREIBUS G, JAGOUTZ E (1984) Mantle chemistry and accretion history of the Earth. In: KRÖNER A, HANSON GN, GOODWIN AM (eds) *Archaean Geochemistry*. Springer-Verlag, Berlin, pp 2–24
- WEBER K, BEHR HJ (1983) Geodynamic interpretation of the Mid-European Variscides. In: MARTIN H, EDER W (eds) *Intracontinental Fold Belts – Case Studies in the Variscan Belt of Europe and the Damara Orogen of Namibia*. Springer, New York, pp 427–469
- WEBER K, VOLLBRECHT A (1986) Kontinentales Tiefbohrprogramm der Bundesrepublik Deutschland. Ergebnisse der Vorerkundungsarbeiten, Lokation Oberpfalz. In: *Second KTB Kolloquium, Seeheim/Odenwald*, pp 1–186
- WIMMENAUER W (1984) Das prävariskische Kristallin im Schwarzwald. *Fortschr Miner* 62: Bh. 2, 69–86
- WIMMENAUER W (1991) Geochemie der metamorphen Sedimentgesteine in der Kontinentalen Tiefbohrung und ihrem Umfeld. *KTB-Report* 91-1: 106–135
- ZULAUF G (1997) Von der Anchizone bis zur Eklogitfazies: Angekippte Krustenprofile als Folge der cadomischen und variscischen Orogenese im Teplá–Barrandium (Böhmische Masse). *Geotekt Forsch* 89: 1–302
- ZULAUF G, FIALA J, FINGER F, LINNEMANN U (2004) Cadomian orogenic imprints in the Bohemian Massif (Austria, the Czech Republic and Germany). *Field Trip Guide Book – B31*. 32nd International Geological Congress, Florence, pp 1–44
- ŽÁČEK V (1994) Garnets and metamorphic evolution of the Teplá Crystalline Complex, Western Bohemia. *Zbl Geol Paläont Teil I*, 7/8: 847–856
- ŽÁČEK V, CHÁB J (1993) Metamorphism in the Teplá Upland, Bohemian Massif, Czech Republic (preliminary report). *Věst Čes geol Úst* 68: 33–37